Mammalian Ykt6 Is a Neuronal SNARE Targeted to a Specialized Compartment by its Profilin-like Amino Terminal Domain

Haruki Hasegawa,* Sara Zinsser* Yeyoung Rhee* Einar Osland Vik-Mo,[†] Svend Davanger,[†] and Jesse C. Hay*[‡]

*University of Michigan, Department of Molecular, Cellular, and Developmental Biology, Ann Arbor, Michigan 48109-1048; and [†]University of Bergen, Department of Anatomy and Cell Biology, and Locus on Neuroscience, Bergen, Norway

SNAREs are required for specific membrane fusion throughout the endomembrane system. Here we report the characterization of rat ykt6, a prenylated SNARE selectively expressed in brain neurons. Immunofluorescence microscopy in neuronal and neuroendocrine cell lines revealed that membrane-associated ykt6 did not colocalize significantly with any conventional markers of endosomes, lysosomes, or the secretory pathway. However, ykt6-containing membranes displayed very minor overlaps with lysosomes and dense-core secretory granules and were similar to lysosomes in buoyant density. Thus, ykt6 appears to be specialized for the trafficking of a unique membrane compartment, perhaps related to lysosomes, involved in aspects of neuronal function. Targeting of this SNARE to the ykt6 compartment was mediated by its profilin-like amino-terminal domain, even in the absence of protein prenylation. Although several other R-SNAREs contain related amino-terminal domains, only the ykt6 version was able to confer the specialized localization. Rat ykt6, which contains an arginine in its SNARE motif zero-layer, was found to behave like other R-SNAREs in its SNARE assembly properties. Interestingly, cytosolic ykt6, constituting more than half of the total cellular pool, appeared to be conformationally inactive for SNARE complex assembly, perhaps indicative of a regulatory mechanism that prevents promiscuous and potentially deleterious SNARE interactions.

INTRODUCTION

SNARE complexes bridge opposing membrane bilayers and appear to mediate specific membrane fusion in the endomembrane system (Sollner *et al.*, 1993; Hay, 2001). Each SNARE complex characterized to date appears to consist of a thermostable parallel helix bundle composed of four heptad repeat-containing SNARE motifs (Sutton *et al.*, 1998; Antonin *et al.*, 2000; Fukuda *et al.*, 2000; Xu *et al.*, 2000; Antonin *et al.*, 2002). A unifying principle is that three of the SNARE motifs are anchored in one membrane and form a target- or "t-SNARE" complex that serves as a binding site for the fourth, vesicle- or "v-SNARE" motif, which is anchored in the opposing membrane. Because the parallel SNARE motifs are anchored via transmembrane domains continuous with the carboxy end of the SNARE motifs, the

zippering up of the v-SNARE motif with the t-SNARE complex positions the two membranes into close apposition and drives lipid mixing and fusion between the opposing bilayers. Interestingly, almost all SNAREs known to be part of a t-SNARE complex contain a glutamine at the conserved "0-layer" position in the center of the helix bundle (called "Q-SNAREs"), whereas the fourth, opposing, v-SNARE motif always contains an arginine at this position ("R-SNAREs"; Fasshauer *et al.*, 1998). Although all SNARE complexes share a common function in membrane fusion catalysis, distinct SNARE complexes function at distinct membrane transport steps.

A great deal has been learned about SNAREs from studies of the yeast endomembrane system, including those involved in ER-to-Golgi, Golgi-to-vacuole, Golgi-to-plasma membrane transport and homotypic vacuole fusion. Most of the yeast SNAREs have mammalian orthologues with similar functions; however, the yeast genome contains 21 recognizable SNAREs, whereas the human genome contains at least 36 (Bock *et al.*, 2001). Similarly, whereas yeast contains only five R-SNAREs (Snc1p, Snc2p, Nyv1p, Sec22p, and

‡ Corresponding author. E-mail address: jessehay@umich.edu.

Ykt6p), mammalian cells contain at least 10 (VAMPs 1, 2, 3, 4, 5, 7, and 8, sec22b, ykt6, and tomosyn). Hence, it appears that mammalian cells must engage in a greater number of SNARE-dependent membrane transport steps, and/or certain mammalian SNAREs have redundant functions. In some cases the demands of multicellularity have necessitated the creation of highly specialized membrane compartments, and the trafficking of these membranes necessitated distinct, tissue-specific SNAREs. Indeed, syntaxin 1A, SNAP-25, and VAMP 2 are mammalian SNAREs specific to regulated exocytic vesicles and have no direct functional homologues in yeast. Likewise, VAMP 5, presumably a plasma membrane SNARE, was found to be present primarily in muscle cells and was induced during myogenesis (Zeng et al., 1998). In addition, syntaxin 17 was found to be enriched in the smooth ER of steroidogenic cells (Steegmaier et al., 2000), and syntaxin 11 may have a specialized trafficking role in the immune system (Prekeris et al., 2000).

Yeast Ykt6p is a prenylated R-SNARE lacking a transmembrane domain (McNew et al., 1997). It was first discovered (Sogaard et al., 1994) as a binding partner of Sed5p, the major syntaxin involved in ER-to-Golgi and intra-Golgi transport. A temperature-sensitive allele of Ykt6p causes secretion of the Golgi-modified form of the normally vacuole-localized carboxypeptidase I, indicating an important role for Ykt6p in biosynthetic transport from the Golgi to the vacuole (Tsui and Banfield, 2000). A later study found that Ykt6p overexpression influenced the vacuolar delivery of carboxypeptidase Y, alkaline phosphatase, and aminopeptidase I, three proteins that utilize distinct vesicular pathways of vacuolar delivery (Dilcher et al., 2001). Thus, Ykt6p appears to be involved in multiple transport steps between the Golgi and vacuole. In addition, Ykt6p has been implicated in ER-to-Golgi (McNew et al., 1997) and Golgi retrograde transport (Lupashin et al., 1997), although these results are difficult to interpret because of the possibility that they could have been indirect effects on the Golgi when Golgi-to-vacuole transport is disrupted. Although a specific localization for Ykt6p in yeast has not been reported, it has been detected on purified vacuoles and has also been shown to be required for homotypic vacuole fusion along with Vam7p, Vam3p, Nyv1p, and Vti1p (Ungermann et al., 1999). Hence, although yeast YKT6 is an essential gene, it does not appear to have a sole, specialized function in yeast. In fact, it appears to be an example of a multifunctional R-SNARE, perhaps partially overlapping in function with other R-SNAREs such as Sec22p and Nyv1p. In support of this idea, Ykt6p was specifically overexpressed in Sec22p-lacking strains and appeared to partially compensate for the Sec22p deletion by participating in ER-to-Golgi SNARE complexes normally containing Sec22p (Liu and Barlowe, 2002).

Yeast Ykt6p contains an independently folded amino-terminal (NT) domain with structural similarity to the NT domains of yeast and mammalian sec22 isoforms and the mammalian lysosomal SNARE VAMP 7. Based on the crystal structure of the mammalian sec22b-NT (Gonzalez et al., 2001) and NMR structure of yeast Ykt6p-NT (Tochio et al., 2001), these domains contain a conserved protein fold similar to that of the actin-binding protein profilin. The features include a slightly curved sheet of five antiparallel β-strands sandwiched between a single α-helix on the concave surface and two antiparallel α-helices on the convex surface. Ho-

mology modeling indicates similar folds for the non-SNARE sec22a and sec22c isoforms and for VAMP 7 (Gonzalez et al., 2001). It seems unlikely that these SNARE NT domains are evolutionarily related to profilin, because the locations of the termini relative to the structural fold are completely different. They also seem unlikely to bind actin because a protruding actin-binding loop on profilin is absent from the SNARE-NT domains. Several other proteins besides SNAREs and profilin contain regulatory domains, called PAS and GAF domains, with a similar overall fold, as well (Borgstahl et al., 1995; Ho et al., 2000). However, the diversity of their binding specificities is too variable to provide useful clues to the function of the SNARE NT domains. In support of a possible autoinhibitory role for the Ykt6p NT domain, mutations in several conserved hydrophobic residues resulted in a modest increase in SNARE complex formation rate (Tochio et al., 2001). However, these results should be interpreted cautiously because removal of the entire msec22b-NT did not measurably affect SNARE complex formation (Gonzalez et al., 2001). Overall, the precise physiological role(s) of the SNARE profilin-like domains has not yet emerged from studies in yeast or mammalian systems.

Because Ykt6p was involved in ER-to-Golgi transport in yeast, we began to characterize the mammalian homolog of Ykt6p, which, we thought, might also be involved in ER-to-Golgi transport. To our surprise, rat ykt6 was not ubiquitously expressed as expected of a SNARE involved in basic secretory trafficking; in fact it was highly enriched only in neurons and was expressed only at very low levels or not at all in other tissues, such as liver, known to have active secretory pathways. Hence, rat ykt6 may have a specialized trafficking function in brain, instead of or in addition to a role in the constitutive secretory pathway. In support of a specialized role, we found that ykt6 had a remarkably unique subcellular localization and did not overlap significantly with endosomal or secretory pathway markers. Punctate ykt6-enriched membranes were spread almost evenly throughout the cytoplasm, resembled lysosomes in buoyant density and colocalized to a very minor degree with synaptotagmin and cathepsin D. Surprisingly, this specialized localization appears to be conferred uniquely by the ykt6 profilin-like domain and does not require protein prenylation. We conclude that protein targeting is an important role of the NT domain and contributes to ykt6 function in a specialized neuronal trafficking pathway.

MATERIALS AND METHODS

Bacterial Expression of GST-Ykt6

An expressed sequence tag (EST) cDNA encoding full-length rat ykt6 (GenBank accession number AA956066), produced by the Program for Rat Gene Discovery (Bonaldo et al., 1996), was obtained from Research Genetics (Huntsville AL), and resequenced at the University of Michigan DNA Sequencing Core. The full-length coding region was amplified by PCR and inserted into pGEX-KG (Guan and Dixon, 1991) using XbaI and SacI restriction sites and transformed into the Escherichia coli strain AB1899. Cultures were grown in LB at 37°C to an optical density of 0.6–0.8, and protein production was induced by the addition of 0.1 mM IPTG at 15°C. The induction was allowed to continue for 3–4 h at 15°C, after which the bacteria were pelleted and resuspended in French Press Buffer (50 mM Tris, pH 8.0, 0.1 M NaCl, 1 mM EDTA, 0.05% Tween 20, 1 mM DTT, 2 μg/ml leupeptin, 4 μg/ml aprotinin, 1 μg/ml pepstatin A,

1 mM phenylmethylsulfonyl fluoride [PMSF]) at 20 ml/liter culture, French Pressed twice, and centrifuged at 20,000 × g for 20 min. The supernatant was then centrifuged at 100,000 × g for 45 min. GST-ykt6 was purified from the resulting supernatant using a glutathione-Sepharose column (Amersham Pharmacia Biotech, Piscataway, NJ), which was eluted with 50 mM Tris, pH 8.0, 20 mM reduced glutathione and 0.1% Triton X-100.

Chicken Polyclonal Anti-Ykt6

Purified GST-ykt6 was dialyzed in PBS, concentrated by ultrafiltration, and emulsified with Freund's adjuvant to immunize chickens. The anti-ykt6 antibody was purified from total chicken IgY by negative and positive purification on a GST- and GST-Ykt6-Sepharose column, respectively. The affinity columns were constructed using CNBr-Sepharose (Amersham Pharmacia) following the manufacturer's instructions. The columns were washed extensively with 10 mM Tris, pH 7.5, plus and minus 0.5 M NaCl, and then the antibody was eluted with 0.1 M glycine, pH 2.5.

Rabbit Polyclonal Anti-DGH Peptide Antibody

The synthetic peptide DGHLSRYQNPREADPMSKC was dissolved in PBS at a concentration of 10 mg/ml and mixed in approximately equal mass with sulfo-SMCC-derivatized keyhole limpet hemocyanin (obtained from and prepared according to Pierce, Rockford, IL) and used for immunization of rabbits with Freund's adjuvant. Anti-DGH antibody was affinity-purified from crude rabbit serum on a column containing covalently linked DGH peptide constructed using Sulfo-Link Gel from Pierce according to the manufacturer's instructions. Antibodies were eluted as above. The serum was first depleted of nonspecific antibodies by passage over an irrelevant peptide affinity column.

Other Antibodies and Probes

Anti-rbet1 mAb 16G6 and anti-membrin polyclonal antibodies were previously described (Hay *et al.*, 1998). Rabbit polyclonal anti-msec13 antibody was generated by immunizing rabbits with bacterially expressed, purified msec13. Rabbit polyclonal anti-GM130 and anti-p115 were a gift from Dr. Martin Lowe (University of Manchester, Great Britain). Monoclonal anti-syntaxin 6 clone 3A10 was a gift from Drs. Jason Bock and Richard Scheller (Genentech Inc., South San Francisco, CA). Rabbit polyclonal anti-EEA1 was a gift from Dr. Vojo Deretic (University of New Mexico). Rabbit polyclonal anti-VAMP 7 was a gift from Dr. Rob Piper (University of Iowa). Anti-syntaxin 13 was a gift from Dr. Rytis Prekeris (University of Colorado Health Science Center, Denver, CO). Rabbit polyclonal anti-cathepsin D was obtained from Upstate Biotechnology (Lake Placid, NY; catalogue number 06-467). Rabbit polyclonal anti-VAMP 2 was obtained from Stressgen (Victoria, BC, Canada; catalogue number VAS-SV006). Monoclonal anti-transferrin receptor was obtained from Zymed (South San Francisco, CA; catalogue number 13-6800). Monoclonal anti–SNAP-25 was obtained from Transduction Labs (Lexington, KY; catalogue number S35020). Monoclonal anti–LAMP-1 (clone 1D4B), anti–LAMP-2 (clone ABL-93), and anti-synaptotagmin (clone mAB 48) were obtained from the Developmental Studies Hybridoma Bank at the University of Iowa. Rabbit polyclonal anti-syntaxin 7 was obtained from Synaptic Systems GmbH (Gottingen, Germany; catalogue number 110-072). Monoclonal anti-GFP was obtained from Covance (Richmond, CA; catalogue number MMS-118P). Anti-myc mAb was produced in our laboratory from tissue culture supernatant from the hybridoma 9E10. Anti–α-tubulin was from Molecular Probes (Eugene, OR; catalogue number A-11126), as was Allexa Fluor 594 phalloidin (catalogue number A-12381) and Texas Red-dextran (catalogue number D-3328).

Membrane Association Experiments

Rat brains were homogenized with a Potter Elvejem device in Homo Buffer (20 mM HEPES, pH 7.0, 0.25 M sucrose, 2 mM EGTA, 2 mM EDTA) supplemented with 1 mM DTT, 2 µg/ml leupeptin, 4 µg/ml aprotinin, 1 µg/ml pepstatin A, and 1 mM phenylmethylsulfonyl fluoride and centrifuged for 15 min at 1000 × g to obtain a postnuclear supernatant (PNS). PNS fractions were then centrifuged at 100,000 × g for 40 min to separate membranes from the cytosol. Analysis of the PNS and 100,000 × g supernatants and pellets are shown in Figure 1. For the membrane extraction studies (see Figure 2), membrane pellets were then rehomogenized in Homo Buffer and repelleted at 100,000 × g to remove residual soluble ykt6. Washed membrane pellets were then resuspended and rehomogenized in the following buffers: Homo Buffer, Homo Buffer containing 1% Triton X-100, Homo Buffer containing 1 M KCl, or 0.2 M sodium carbonate, pH 11.4. After 30 min of agitation, the membrane suspensions were centrifuged at 100,000 × g for 40 min, and the supernatants and pellets were analyzed by SDS-PAGE and immunoblotting. For Triton X-114 partitioning experiments, the protein concentrations of the 100,000 × g supernatant (cytosol) and a resuspended washed membrane pellet were determined with the Bio-Rad Protein Assay (Hercules, CA). A 10% (wt/vol) Triton X-114 solution in PBS was added to these fractions so that there was 10 mg of detergent per mg of protein. These solutions were incubated with tumbling at 4°C for 1 h and centrifuged at 20,000 × g for 10 min at 4°C to remove any insoluble material. After removing the supernatants to fresh tubes, the solutions were clouded at 37°C for 10 min. They were then centrifuged at room temperature at 20,000 × g for 10 min to separate the aqueous and detergent layers. After removing the aqueous layer to a fresh tube, the protein in both phases was precipitated with 3 volumes of ice-cold acetone. The tubes were centrifuged at 100,000 × g for 20 min to pellet the precipitated protein, the acetone was removed, and the pellets were dissolved in SDS sample buffer for SDS-PAGE and immunoblotting with control and anti-ykt6 antibodies.

Similar experiments were carried out with PC12 cells transfected with myc-ykt6 constructs (see Figure 10). PC12 cells were harvested using HBSS containing 1 mM EDTA. The cells were collected by centrifugation, washed, and swelled with 10 mM HEPES, pH 7.3, 18 mM potassium acetate, and resuspended in Homo Buffer containing 1 mM DTT, 10 µg/ml aprotinin, 4 µg/ml leupeptin, 1 µg/ml pepstatin, and 1 mM 4-(2-aminoethyl)bezenesulfonyl fluoride (AEBSF). Cells were then homogenized using ~20 strokes in a glass Dounce homogenizer, and a postnuclear supernatant was collected after 10 min of centrifugation at 720 × g. Postnuclear supernatants were centrifuged at 100,000 × g for 1 h, and the supernatant (cytosol) was removed and saved. The pellet was resuspended and washed with Homo Buffer and recentrifuged, and the supernatant discarded. Equal proportions of the cytosol and pellet fractions were analyzed by immunoblotting. Triton X-114 partitioning of PC12 cell cytosols was similar to those described above except that the final Triton X-114 concentration used was 2%, irrespective of protein concentration (which was much lower in these experiments).

Tissue Distribution

Freshly dissected rat tissues were placed in approximately four volumes of Homo Buffer containing protease inhibitors and immediately homogenized using a Polytron homogenizer (Brinkmann, Westbury, NY) on maximum setting. Protein concentrations of the various tissue homogenates were determined with the Bio-Rad protein assay, and samples of each tissue were prepared in SDS-PAGE sample buffer at equal protein concentrations. Gel samples were then analyzed by SDS-PAGE and immunoblotting with anti-ykt6, anti-DGH, and control antibodies.

Immunofluorescence Microscopy

NG108 cells obtained from American Type Culture Collection (Manassas, VA) were maintained in DMEM medium lacking sodium
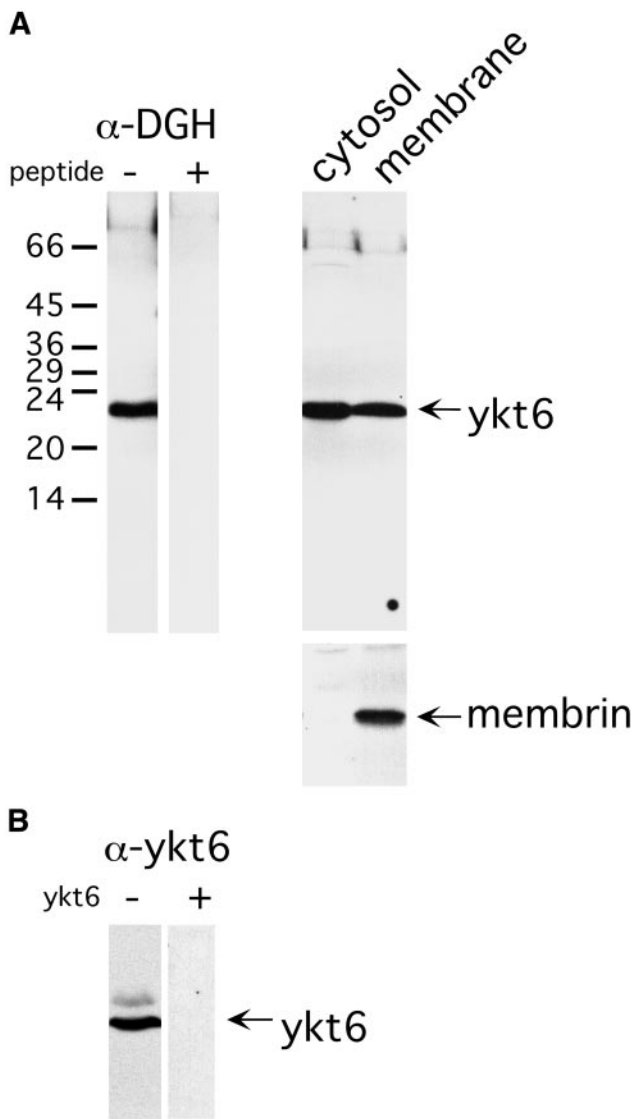
A

B

Figure 1. Polyclonal antibodies recognizing rat brain ykt6. Rat brain postnuclear supernatant was electrophoresed on 12% SDS-PAGE, transferred to nitrocellulose, and immunoblotted with affinity-purified rabbit anti-DGH peptide-specific antibody (A) or chicken anti-ykt6 antibody (B). Competitor DGH peptide or purified ykt6 was included as indicated to demonstrate specificity. The right hand panel in A shows immunoblotting of postnuclear supernatant fractions that were centrifuged at $100,000 \times g$, to generate a supernatant ("cytosol") or a pellet ("membranes") fraction. Panel A, lower right, shows the same blot probed with antibodies against an integral membrane protein, membrin, to demonstrate that the separation of membranes and cytosol was complete. As seen in B, sometimes a faint apparently cross-reactive band was observed running slightly slower than ykt6. In other blots (e.g., Figures 2 and 3), it was not detected.

pyruvate and containing 4 mg/L glucose, 4 mg/L pyroxidine-HCl, 0.1 mM hypoxanthene, 400 nM aminopterin, 0.016 mM thymidine, 3.7 g/L sodium bicarbonate, and 10 percent fetal calf serum, without antibiotics. NRK, FAO, and HepG2 cells were cultured in
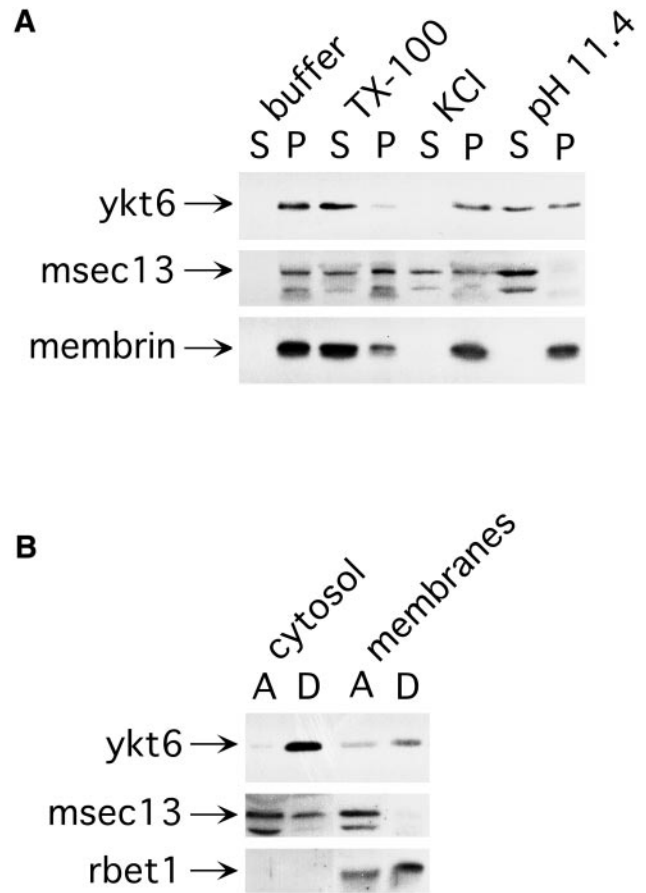
A

B

Figure 2. Rat brain ykt6 behaves like a prenylated membrane protein. (A) Membrane extractions. Rat brain membrane fractions were resuspended in plain buffer, buffer containing Triton X-100, buffer containing 1 M KCl, or carbonate buffer, pH 11.4, as indicated above the lanes. After agitation, the membranes were centrifuged at $100,000 \times g$ and the supernatants (S) and pellets (P) were analyzed by SDS-PAGE and immunoblotting with antibodies against ykt6, the peripheral membrane protein msec13, and the integral membrane protein membrin. (B) Detergent partitioning. Rat brain cytosol and membrane fractions were solubilized with Triton X-114, after which the detergent was phase-separated into aqueous (A) and detergent (D) phases. The phases were then analyzed by SDS-PAGE and immunoblotting with antibodies against ykt6, the peripheral membrane protein msec13, and the integral membrane protein membrin. Note that the total yield of ykt6 in the membrane partitioning is significantly lower than that in cytosol partitioning. This was due to the fact that a significant portion of membrane-associated ykt6 was insoluble in Triton X-114; Triton X-114-insoluble material was removed by centrifugation before partitioning.

DMEM high glucose containing 10% fetal calf serum and penicillin-streptomycin. PC12 cells were cultured in DMEM high glucose containing 5% equine serum and 5% iron-supplemented calf serum, lacking antibiotics. For microscopy, all cells were plated on poly-lysine–treated glass coverslips in standard six-well dishes at a density of ~100,000–500,000 cells per well.

Cells on coverslips were fixed with 0.1 M sodium phosphate, pH 7.0, 2% paraformaldehyde, and 0.05% Triton X-100, for 30 min at room temperature, and quenched in PBS containing 0.1 M glycine twice for 10 min each. Fixed cells were then incubated with perme-

abilization buffer (0.4% saponin, 1% BSA, 2% normal goat serum in PBS) for 15 min, followed by incubation in primary antibody in permeabilization buffer for 1 h. After three washes with permeabilization buffer, cells were incubated with secondary antibody in the same buffer for 30 min. Secondary antibodies were usually FITC- and Texas Red–conjugated and purchased from Jackson ImmunoResearch (West Grove, PA). For LAMP-1 and -2 staining we used Cy3-conjugated goat anti-rat secondary. After the secondary antibody incubation, coverslips were washed with permeabilization buffer three further times, and the coverslips were mounted using Vectashield mounting medium (Vector Laboratories, Burlingame, CA) and sealed with nail polish. Slides were analyzed using a Nikon E800 microscope (Garden City, NY) using a 100× CFI Plan Apo or 60× CFI Plan Apo objective. Optics included standard FITC and Texas Red excitation/emission filter sets that allowed negligible cross-talk between Texas Red and FITC or GFP. Images were collected using a Hamamatsu ORCA 2 digital camera (Bridgewater, NJ) and Improvision Openlab 2 software (Lexington, MA). Images were imported into Adobe Photoshop (San Jose, CA) to be cropped and then arranged and labeled using Deneba Canvas (Miami, FL). For deconvolution, we used separate excitation and emission filter wheels equipped with GFP and dsRed-optimized filters and captured images every 0.2 μm from the top to bottom of the cells (for PC12 cells, this was ~30 z-sections). We then deconvolved the stack of images using the Openlab 3D Restoration algorithm, which removes no light from the image stack, only redistributes it to its calculated point of origin, and involves absolutely no arbitrary user inputs. We present only single optical sections of deconvolved image stacks.

myc-ykt6 Expression Constructs

Amino acid residues 1–198, 1–193, and 1–137 of rat ykt6 were amplified by PCR using specific forward primers containing *Sac*II and specific reverse primers including a stop codon followed by *Xba*I. PCR products were cut with *Sac*II and *Xba*I, purified, and subcloned into pCMV-myc (Hay *et al.*, 1997) at *Sac*II/*Xba*I sites to generate myc-rykt6, myc-rykt6 ΔCCAIM, and myc-rykt6-NT, respectively. myc-rykt6 CC194,195AA was produced by PCR-based site-directed mutagenesis using myc-rykt6 as template. Amino acid residues 137–198 of rat ykt6 was PCR-amplified using a *Sac*II-*Kas*I-*Nhe*I containing specific forward primer and a specific reverse primer containing a stop codon followed by *Xba*I. The purified *Sac*II-*Xba*I fragment was subcloned into the *Sac*II/*Xba*I sites of pCMV-myc as before to generate myc-rykt6 ΔNT. Amino acid residues 1–133 of mouse sec22b were amplified by using a *Sac*II containing specific forward primer and a *Nhe*I containing specific reverse primer. The *Sac*II-*Nhe*I fragment was purified and subcloned to *Sac*II-*Nhe*I of myc-rykt6 ΔNT to generate myc-rykt6 (sec22b-NT). Full-length and the first 139 amino acid residues of yeast Ykt6p were PCR-amplified using specific forward primers containing *Sac*II and specific reverse primers with a stop codon followed by *Nhe*I. *Sac*II-*Nhe*I fragments were purified and subcloned into pCMV-myc at compatible *Sac*II/*Xba*I sites to create myc-yYkt6p and myc-yYkt6p-NT. For each construct, the correct sequence of the entire open reading frame was confirmed at the University of Michigan Sequencing Core. PC12 cells were transfected using Lipofectamine 2000 (Invitrogen, Carlsbad, CA). Transfected cells on coverslips were fixed ~48 h after transfection and were stained as described above. Other dishes of transfected PC12 cells were lysed directly in SDS sample buffer and analyzed by immunoblotting (see Figure 10B) or harvested with HBSS for biochemical fractionation (see Membrane Association Studies or Subcellular Fractionation).

Subcellular Fractionation

Eight confluent 10-cm plates of PC12 cells were harvested by pipetting using HBSS containing 1 mM EDTA. The cells were collected by centrifugation and resuspended in 0.5 ml Optiprep (Sigma Chemical Co., St. Louis, MO) diluent (0.25 M sorbitol, 10 mM HEPES, pH 7.4, 1 mM EDTA) containing 1 mM DTT, 4 μg/ml aprotinin, 10 μg/ml leupeptin, 1 μg/ml pepstatin, and 1 mM AEBSF. Cells were then homogenized using 30 strokes in a glass Dounce homogenizer, and a postnuclear supernatant was collected after 10 min of centrifugation at 720 × *g*. The postnuclear supernatant was layered on top of a density barrier consisting of 2 ml of 2% Optiprep (Sigma) resting on a 0.5-ml pad of 50% Optiprep, made up in Optiprep diluent. The tube was topped off with Optiprep diluent and centrifuged at 35,000 rpm (100,000 × *g* at r_{av}) for 30 min in a Beckman MLS-50 rotor (Fullerton, CA). Soluble proteins remained in the sample layer while membranes concentrated at the 2%/50% Optiprep interface. The 2/50 interface was collected, adjusted to 200 μl of 28% Optiprep with the aid of a refractometer, and layered underneath a continuous 5–25% Optiprep gradient made up in Optiprep diluent. This gradient was centrifuged at 43,000 rpm (150,000 × *g* at r_{av}) for 1.5 h in an MLS-50 rotor. The gradient was unloaded from the bottom using a peristaltic pump, and the membranes were concentrated using Centricon-10 devices (Millipore, Bedford, MA) before analysis by SDS-PAGE and immunoblotting with various antibodies.

Light Microscopic Immunocytochemistry of Vibratome Sections

Rats were deeply anesthetized with sodium pentobarbital (50 mg/kg) and subjected to transcardiac perfusion with fixative (a mixture of 2% formaldehyde and 0.2% picric acid), after a brief flush of 2% dextran (MW 70,000) in sodium phosphate buffer (pH 7.4; PB), all solutions 4°C. The fixative was bicarbonate-buffered, initially at pH 6.0, and then after 5 min with a shift to pH 10.5 (pH shift protocol). The brain was left in situ overnight at 4°C before dissection and sectioning with a Vibratome at 50 μm. Sections were immunostained with the chicken anti-ykt6 antibody at 1:100 and 1:30. Briefly, the sections were incubated sequentially in 1) ethanolamine (1 M in PB); 2) blocking buffer (BB; 10% normal sheep serum and 1% BSA in PB); 3) primary antibody in BB overnight at 4°C; 4) BB; 5) secondary antibody 1:100 in BB (biotinylated sheep anti-mouse Ig; Amersham); 6) BB; 7) horseradish peroxidase complex 1:100 in BB (streptavidin conjugated; Amersham); and 8) diaminobenzidine (0.05%) and hydrogen peroxide (0.01%; both from Sigma) in PB (3–4 min). Sections were rinsed in PB between incubations. The sections were examined with a Zeiss Axiophot microscope (Thornwood, NY) and photographic negatives were digitized with an Agfa Arcus II scanner (Orangeburg, NY).

SNARE Complex Assembly Assay

ER/Golgi SNAREs (sec22b, syntaxin 5, membrin, and rbet 1) were expressed in bacteria and purified by methods described previously (Xu *et al.*, 2000). GST-ykt6 was produced as described above, cleaved free of GST with thrombin (Sigma Chemical CO.; catalogue number T 1063), and separated from GST on Mono Q anion exchange chromatography (Amersham). All proteins were dialyzed in Buffer A (20 mM HEPES, pH 7.2, 0.15 M KCl, 2 mM EDTA, 5% glycerol) and supplemented with 1 mM DTT, 2 μg/ml leupeptin, 4 μg/ml aprotinin, and 1 μg/ml pepstatin A. Assembly reactions were set up in buffer A containing 0.1% Triton X-100, with all proteins present at ~2 μM, and incubated on ice overnight. They were then gel filtered on Superdex 200 as previously described (Xu *et al.*, 2000). Fractions collected from each gel filtered reaction were analyzed by SDS-PAGE and immunoblotting. For the assembly reactions shown in Figure 14, using partially purified brain ykt6, the ykt6 concentration in the final assembly reaction was ~100-fold lower than that shown in Figure 13. In this case, the purified recombinant ykt6 was diluted before addition such that approximately equal ykt6 concentrations were present in the cytosolic and recombinant assembly reactions. Also in this case, the gel filtration

fractions had to be acetone-precipitated before immunoblotting to be able to detect ykt6 in a high-molecular-weight complex.

Partial Purification of Rat Brain Cytosolic ykt6

Twenty-five frozen unstripped rat brains (Pel Freeze Biologicals, Rogers, AR) were thawed on ice and homogenized with a Polytron (Brinkmann, Westbury, NY) in Homo Buffer with protease inhibitors (see above). After homogenization, large membranes and debris were removed by centrifugation at $27,000 \times g$ for 15 min in a Sorvall SS-34 rotor (Newton, CT), and then this supernatant was centrifuged at $100,000 \times g$ for 90 min in a Beckman MLA-80 rotor. The final supernatant was passed over a 30-ml column of Q-Sepharose (Pharmacia, Piscataway, NJ) at 0.5 ml/min, which was washed down to baseline absorbance with 20 mM Tris, 1 mM EGTA, pH 7.6, and then eluted with a gradient to 1 M KCl in the same buffer. Immunoblotting revealed that the vast majority of ykt6 was found in the flowthrough. Because we also needed the flowthrough for another unrelated purification, only about one third of the total ykt6 pool was carried forward in the ykt6 purification. The selected flowthrough fractions were dialyzed into 50 mM sodium phosphate, pH 6.0, and passed over a 1 ml Mono S column (Pharmacia) at 1 ml/min. The Mono S was washed to baseline and then eluted with a gradient to 1 M NaCl in the same buffer. Again, the vast majority of ykt6 was present in the flowthrough, although many major contaminant proteins had been removed. The Mono S flowthrough was dialyzed into 50 mM sodium phosphate, pH 7.3, and loaded onto a 10 ml Biogel HT column (Bio-Rad) at 0.4 ml/min, washed to baseline, and eluted with a gradient to 0.4 M potassium phosphate, pH 7.3. Immunoblotting revealed that all of the ykt6 was present in a sharp peak at ~175 mM phosphate, resulting in an ~10-fold specific enrichment over the loaded fraction. The HT peak fractions were then concentrated in a Centricon-3 device (Amicon, Beverly, MA), and gel-filtered on a 100 ml Superose 12 column in Buffer A (see above) lacking detergent at 1 ml/min. Ykt6 eluted in a sharp peak at approximately the molecular weight expected for monomeric ykt6, resulting in an enrichment of ~10-fold over the loaded material. Two adjacent peak fractions were then pooled and used for the analyses shown in Figures 14 and 15.

Velocity Gradient Sedimentation

Four milliliter continuous 5–30% glycerol gradients were prepared in polycarbonate tubes (Beckman no. 349622) in Buffer A plus 0.2% Triton X-100 and overlayed with ~200 μl of sample. Gradients were centrifuged for 20–30 h at maximum speed in an MLS-50 rotor at 4°C with slow acceleration/deceleration and fractionated into 350 μl samples by hand pipetting from the top. Samples were acetone-precipitated and analyzed by SDS-PAGE and immunoblotting with anti-ykt6 antisera. Calibration proteins were run in identical gradients and analyzed by SDS-PAGE and Coomassie staining.

Protease Sensitivity Analysis

Samples to be protease K–treated were either appropriately diluted purified recombinant ykt6, rat brain cytosol, or rat brain cytosol depleted of endogenous ykt6 and then supplemented with an equivalent amount of purified recombinant ykt6. To prepare ykt6-depleted cytosol, 100 μl of cytosol (~1 mg protein) was incubated with 2.9 μg of affinity-purified chicken anti-ykt6 for 2 h and then depleted of antibody using 10 μl of 50% protein A-Sepharose (Pharmacia) that had been coated with 10 mg rabbit anti-chicken IgG per milliliter of packed beads. The nondepleted cytosol was treated in the identical manner, except that no primary antibody was added. Protease K was dissolved in Homo Buffer at 1 mg/ml immediately before the experiment. Aliquots of 10 μl of cytosol or purified proteins in Homo Buffer lacking protease inhibitors were supplemented with 1 μl of protease K, incubated for the indicated times on ice, and then treated with 0.5 μl of 0.1 M PMSF, one volume of 2×

SDS sample buffer, boiling, and SDS-PAGE followed by immunoblotting with anti-ykt6 antisera.

RESULTS

Rat ykt6 cDNA

An EST encoding full-length rat ykt6 (GenBank accession number AA956066) was obtained from the Program for Rat Gene Discovery (Bonaldo *et al.*, 1996) and resequenced at the University of Michigan Sequencing Core. The encoded protein was almost identical to the rat ykt6 cDNA isolated earlier (GenBank accession number AF033027; Catchpoole and Wanjin, 1999) but differed at four amino acid positions (L at residue 9 in the previous sequence was F in our sequence; K at residue 14 in the previous sequence was P in our sequence; Q at residue 100 in the previous sequence was E in our sequence; T at residue 107 in the previous sequence was R in our sequence). We compared *Saccharomyces cerevisiae*, *Candida albicans*, *Saccharomyces pombe*, mouse, human, *Xenopus*, *Drosophila*, tobacco, and *Arabidopsis* ykt6 homologues at those positions and found that in the first two cases, either amino acid occurred in other organisms. In the second two cases, however, our sequence agreed with at least four other organisms, whereas the previous sequence was an outlier. Thus, the first two amino acid differences might be due to rat polymorphism, whereas the last two may represent sequencing errors in the earlier rat sequence.

Antibodies to Rat ykt6

Antibodies against the vertebrate ykt6 protein have been technically difficult to produce. For antibodies that were excellent in immunoblotting applications, we immunized rabbits with the peptide DGHLSRYQNPREADPMSKC conjugated to keyhole limpet hemacyanin (see MATERIALS AND METHODS). This peptide contains amino acids 124–141 and overlaps with the amino end of the SNARE motif of rat ykt6. Affinity-purified rabbit antisera generated from this peptide, termed "anti-DGH," recognized a single band of ~23 kDa in rat brain postnuclear supernatant that was completely blocked by addition of the DGH peptide (Figure 1A). Centrifugation of postnuclear supernatant at $100,000 \times g$ to generate cytosol and membrane fractions demonstrated that ~50–70% of the cellular ykt6 was cytosolic (Figure 1A). In contrast, in the same samples, 100% of the membrin, an integral membrane ER/Golgi Q-SNARE, was membrane-associated. A second antibody that was useful for immunoblotting as well as light microscopy was generated by immunizing chickens with bacterially expressed GST-ykt6, including full-length ykt6, amino acids 1–198. The resulting antibody, termed "anti-ykt6" was purified from total chicken IgY by negative purification on GST-Sepharose followed by positive purification on GST-ykt6-Sepharose (see MATERIALS AND METHODS). Anti-ykt6 also specifically recognized the 23-kDa band in rat brain postnuclear supernatant and was completely blocked by addition of purified GST-ykt6 (Figure 1B).

Rat ykt6 Appears to be Membrane-anchored by Protein Prenylation

Neither yeast nor mammalian ykt6 contain predicted transmembrane domains, but both contain predicted prenylation

sites at their carboxy termini (CCIIM in yeast and CCAIM in rat). Consistent with membrane attachment through prenylation, the yeast Ykt6p behaves as an integral membrane protein and exhibits pronounced hydrophobicity in detergent partitioning experiments (McNew *et al.*, 1997). Likewise, the one previous report on mammalian ykt6 found that it behaved as an integral membrane protein on liver membranes (Zhang and Hong, 2001). However, because we did not find evidence of significant ykt6 in liver (see below), we revisited these experiments with brain, perhaps a functionally more relevant source of ykt6. As shown in Figure 2A, membrane-associated rat brain ykt6 exhibited a strength of membrane attachment in between that of an integral membrane protein (membrin) and a peripheral membrane protein (msec13). Ykt6 was completely extracted by Triton X-100, was extracted not at all by 1 M KCl and was partially extracted by carbonate buffer, pH 11.4. In contrast, msec13 was significantly extracted by all the treatments, whereas membrin was extracted with Triton and was not affected by the other treatments. These results are consistent with ykt6 being firmly embedded in the membrane core, though not to the degree of a single-pass transmembrane protein. To determine whether the hydrophobicity of ykt6 was also consistent with prenylation, we performed Triton X-114 phase partitioning analysis. As shown in Figure 2B, the majority of Triton X-114-soluble ykt6 distributed into the detergent phase, as expected of hydrophobic proteins and demonstrated by rbet1. On the other hand, the majority of msec13, a peripheral membrane protein, was recovered in the aqueous phase. Interestingly, in confirmation of what was discovered for yeast Ykt6p (McNew *et al.*, 1997), even soluble rat ykt6 partitioned into the detergent phase, indicating that cytosolic ykt6 is also likely prenylated.

Rat ykt6 Is Expressed Selectively in Brain

The tissue distribution of vertebrate SNAREs is an important clue to their function. Given the function of yeast Ykt6p in fundamental transport pathways such as ER-to-Golgi and Golgi-to-vacuole transport (McNew *et al.*, 1997; Dilcher *et al.*, 2001; Tochio *et al.*, 2001), we expected rat ykt6 to exhibit a broad distribution and to be especially enriched in several tissues with an active secretory pathway, such as liver, spleen, and brain. To our surprise, when total extracts of rat tissue were analyzed by immunoblotting using anti-ykt6 antibody, a normal exposure of the blot demonstrated that ykt6 was *only* detected in brain (Figure 3, top panel). Other rat tissues were not underrepresented on the blot because an anti-membrin antibody using a comparable exposure demonstrated that membrin was present in roughly equivalent amounts in brain, spleen, kidney, and liver (Figure 3, second panel), and just visible in skeletal muscle and heart. In addition, Coomassie blue staining of an identical gel before transfer to nitrocellulose demonstrated that comparable protein was loaded in each lane (Figure 3, third panel). On saturating the exposure of the same ykt6 blot, the ykt6 band could be detected at much lower levels in spleen, lung, and kidney; however, ykt6 was still not detectable in heart, muscle, or liver (Figure 3, bottom panel). The selective expression of ykt6 in brain was not a peculiarity of the anti-ykt6 antibody, because the anti-DGH antibody gave comparable results (unpublished data). Likewise, we repeated the experiment with a different individual rat and found virtually
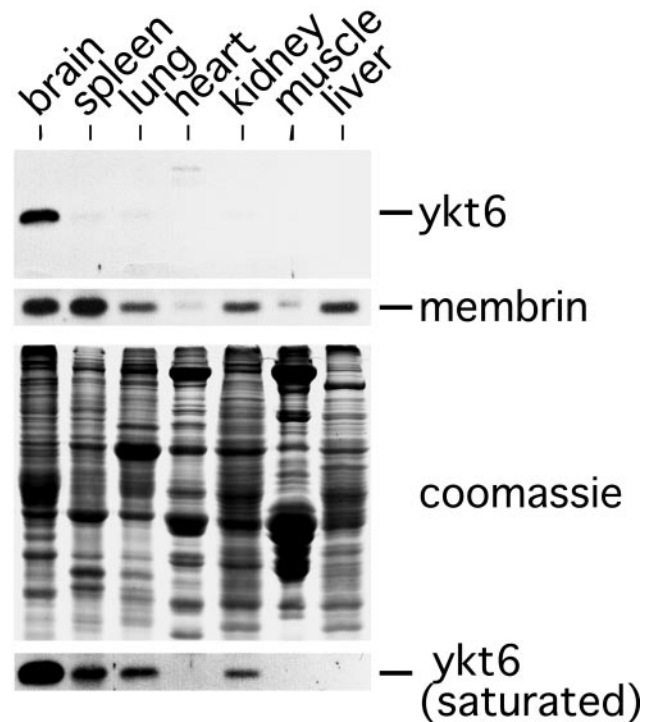

Figure 3. Rat ykt6 is expressed selectively in brain. Freshly dissected rat tissues were homogenized and analyzed on two identical SDS gels; one was stained with Coomassie blue and the other was immunoblotted consecutively with anti-ykt6 antibody and anti-membrin antibody. Detection was with enhanced chemiluminescence. Top two panels show normal (not light) exposures. Bottom panel shows a super-saturating exposure of the anti-ykt6–decorated blot. Similar results for ykt6 on this blot were obtained using the anti-DGH antibody (unpublished data) or using a different blot from a different individual rat (unpublished data).

identical results (unpublished data). The strikingly selective expression of rat ykt6 in brain suggests that ykt6 is specialized for a transport step that is enhanced in or specific to brain. However, it does not eliminate a possible role in more general trafficking steps in other tissues where ykt6 is expressed.

Rat ykt6 Displays a Dispersed Vesicular Localization in Cultured Neuronal and Neuroendocrine Cell Lines

A previous study found that rat ykt6 was associated with the Golgi in NRK cells (Zhang and Hong, 2001). However, because some of our results on rat ykt6 did not agree with this report (see DISCUSSION), we independently determined the intracellular localization of ykt6 by immunofluorescence microscopy. Immunostaining of several cultured cell lines with chicken anti-ykt6 antibody produced a dispersed spotty pattern of cytoplasmic fluorescence, with no particular accumulation of spotty structures in the perinuclear region (unpublished data). The density of staining structures varied dramatically, with the rat neuroendocrine cell line PC12 and the rat-mouse neuroblastoma-glioma cell
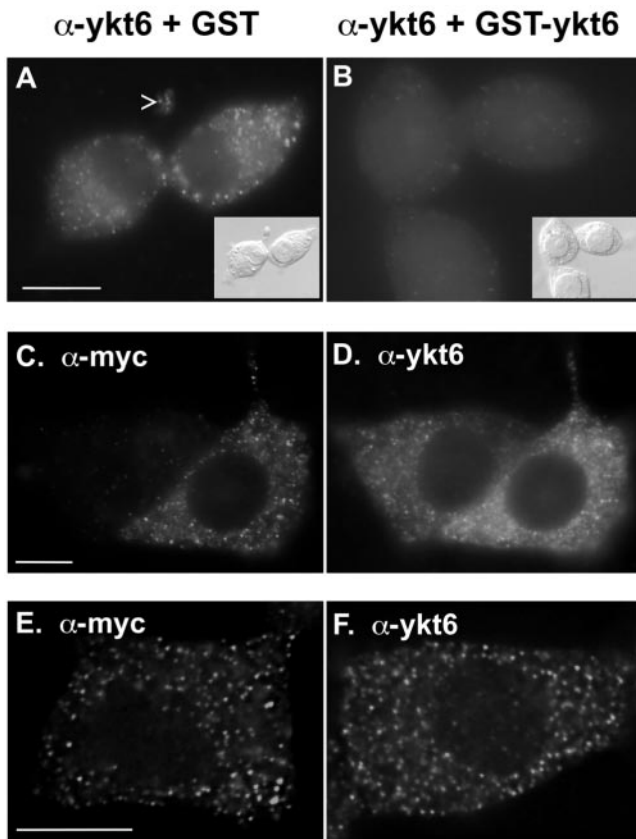
Figure 4. Specificity of punctate ykt6 staining in PC12 cells. (A and B) Punctate ykt6 staining is blocked by ykt6 protein. PC12 cells were fixed and stained with anti-ykt6 antibody and FITC-labeled anti-chicken secondary antibody. (A) Staining was performed in the presence of purified GST. (B) Staining was performed in the presence of an equal concentration of purified GST-ykt6. (C and D) PC12 cells were transfected with myc-rykt6 and stained with either anti-myc (C) or anti-ykt6 (D) antisera. (E and F) Single deconvolved optical sections of different PC12 cells either transfected with myc-rykt6 and stained with anti-myc antibodies (E) or not transfected and stained with anti-ykt6 (F). Insets show DIC staining for selected panels. Arrowhead in A demonstrates that ykt6 vesicles are present in neurite terminals. Bars, 10 μm.

line ng108 (Hamprecht, 1977), giving far more staining than normal rat kidney cells (NRK), and rat FAO hepatoma cells (Witters *et al.*, 1988). Staining was not detected in the human hepatoma cell line, HepG2. Immunoblotting of extracts of the same cell lines revealed a remarkable correlation between the amount of expressed ykt6 and the number of spotty structures seen by immunofluorescence (unpublished data). Because the putative ykt6 staining did not appear to represent Golgi membranes as previously suggested (Zhang and Hong, 2001), we validated our ykt6 staining pattern with several additional experiments. As shown in Figure 4, A and B, the vesicular anti-ykt6 pattern in PC12 cells was completely blocked by purified GST-ykt6 but was not affected by equal concentrations of GST. In addition, when PC12 cells were transfected with myc-ykt6, anti-myc staining of transfected cells gave a pattern very similar to what is

seen with endogenous ykt6 staining (Figure 4, C and D). Note that the anti-ykt6 antibody easily detects transfected cells overexpressing ykt6. In the overexpressing cells, the staining is brighter but similar in nature to that of neighboring untransfected cells (Figure 4D). Approximately 55% of structures discernibly stained with anti-myc antibody were also positive with anti-ykt6, and likewise ~60% of anti-ykt6–staining spots were positive with anti-myc. However, because not all anti-myc spots were positive for anti-ykt6, the staining with at least one of the antibodies must have been incomplete, and it is not possible to assess the degree to which myc-ykt6 and endogenous ykt6 colocalized. Figure 4, F and E, show close-up deconvolved images of endogenous ykt6 stained with anti-ykt6 and recombinant myc-ykt6 stained with anti-myc, respectively, in different cells, for comparison. Figure 4, C–F, indicates that the anti-ykt6 antibody stains both endogenous and recombinant ykt6. In a later experiment (see Figure 10, J–L), we definitively confirmed the authenticity of the chicken anti-ykt6 endogenous staining pattern because recombinant yeast myc-Ykt6p, stained with anti-myc, extensively colocalized with endogenous rat ykt6 stained with chicken anti-rat ykt6, even though chicken anti-rat ykt6 does not react with yeast Ykt6p.

Although we detected much apparently membrane-associated ykt6, relatively little diffuse cytosolic ykt6 was detected, even though >50% of the protein is soluble in fractionation experiments (Figure 1). This was true for both anti-ykt6 as well as anti-myc staining of ykt6 and myc-ykt6 and was not an artifact of paraformaldehyde fixation, because methanol fixation produced very similar staining patterns (unpublished data). There are two likely explanations for this apparent discrepancy. First and most likely, the concentration of ykt6 on its target membrane would be much higher than in the cytosol, and thus might drive much higher antibody labeling. Second, the cytosolic pool of ykt6 is likely found in a distinct conformation and/or associated with different proteins, and the staining epitope(s) may be sensitive to this difference.

Rat ykt6 Does Not Colocalize Significantly with Markers of Secretory Organelles, Endosomal Subcompartments, or Lysosomes

To get clues to the specialized membrane trafficking role of ykt6 in brain, we attempted to identify the ykt6-enriched vesicular membranes in PC12 and ng108 cell lines. As anticipated, there was no similarity between Golgi staining with anti-GM130 and staining with anti-ykt6 (Figure 5, A–C). In fact, one of the distinguishing characteristics of ykt6 staining is that unlike Golgi, TGN, and certain endosomes, there was rarely a pronounced peri-nuclear or juxta-nuclear staining pattern. The ykt6 structures are usually almost uniformly distributed through the cytoplasm and often extend into larger neurites when present (e.g., see Figure 4A, arrowhead, and Figure 5I, detail). We also did not observe overlap between ykt6 and the spotty ER exit sites and Golgi-centric VTCs containing rbet1 (Hay *et al.*, 1997; Figure 5, D–F). The large (~0.5 μm) ykt6-containing spots looked like they could be post-Golgi vesicles such as large dense-core secretory granules. Thus, we costained ykt6 with VAMP2 and synaptotagmin I. VAMP2 displayed very little if any overlap with ykt6 (Figure 5, G–I). Note in Figure 5I that both ykt6 and
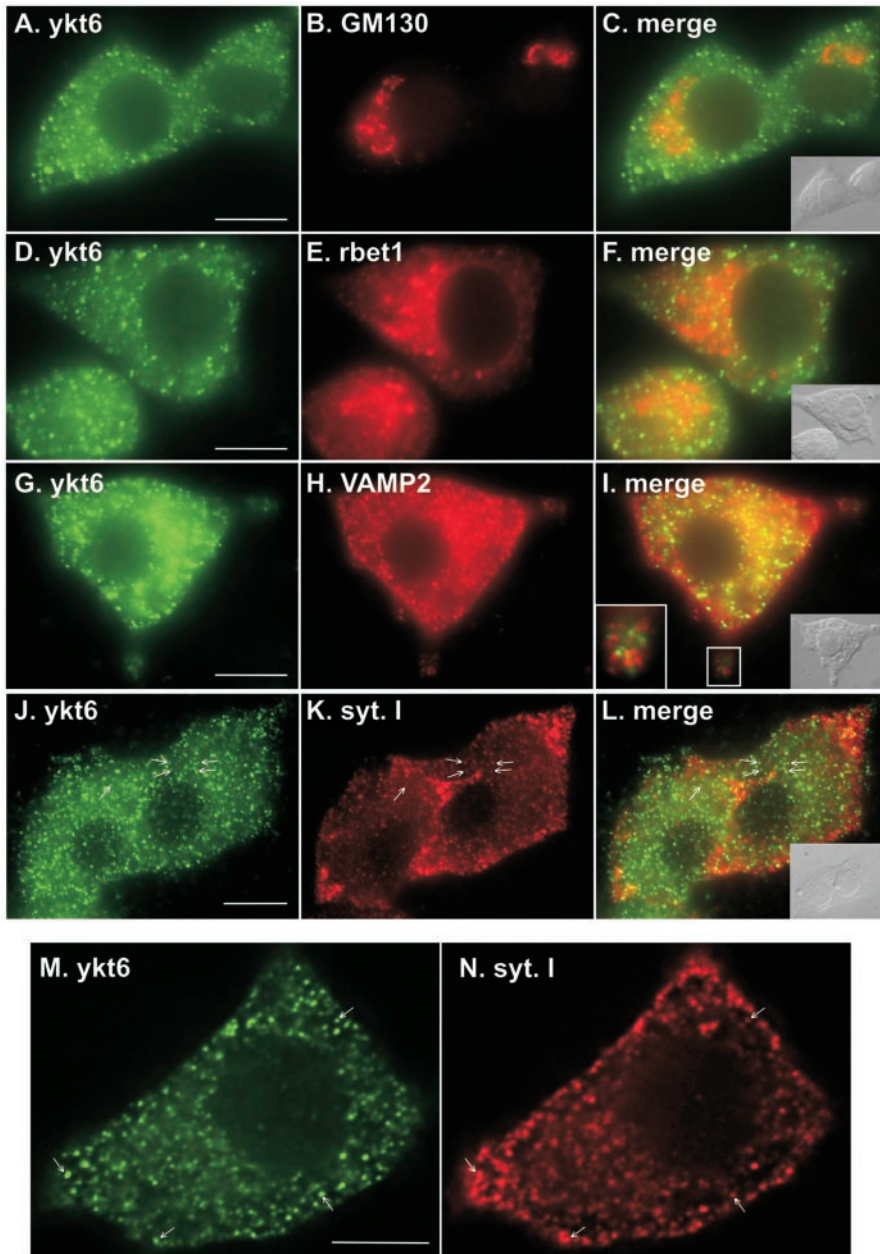
Figure 5. Ykt6-containing membranes do not overlap significantly with markers of the secretory pathway. PC12 cells were fixed and stained with anti-ykt6 antibodies and FITC-labeled secondary antibodies (A, D, G, J, and M) and costained with the following primary antibodies followed by Texas Red–labeled secondary antibodies: GM130 (B), rbet1 (E), VAMP 2 (H) and synaptotagmin I (K and N). Green and red images from the same field were merged (C, F, I, and L). (M and N) Single deconvolved optical sections. Insets show DIC images of the respective fields. Detail in I shows a neurite terminal containing distinct, ykt6- and VAMP2-containing structures. Arrows in J–N point to the few colocalizing spots. Bars, 10 μm.

VAMP2 are present in the swollen terminals of neurites; however, the two kinds of structures were entirely distinct. Synaptotagmin was present in large puncta most concentrated in a ring just under the plasma membrane and thus did not generally overlap with the more evenly distributed ykt6 structures (Figure 5, J–L). However, we consistently saw a very small percentage of synaptotagmin-positive structures that overlapped with ykt6 (see arrows). Although this was only a few clear spots per cell, it was not merely due to the superposition of distinct structures, because deconvolved 0.2-μm optical sections also displayed approximately the same degree of spot overlap (Figure 5, M and N). The two kinds of structures may have shared a common origin

compartment or intermixed to a degree in their lifecycle, but were clearly distinct overall.

Given the very spotty localization of membrane-associated ykt6, and the role of yeast Ykt6p in trafficking to the vacuole, we focused significant attention on known markers of endosomal compartments. Although qualitatively similar in appearance, neither the specific early endosome marker EEA1 (Figure 6, A–C) nor the recycling endosome markers transferrin receptor (Figure 6, D–F) and VAMP 2 (Figure 5, G–I), which appears to be partially endosomal in PC12 cells, overlapped with ykt6. Some yellow areas were observed in merged images (e.g., see Figure 6F), but these were in the central area near the nucleus where the cell is thickest. And
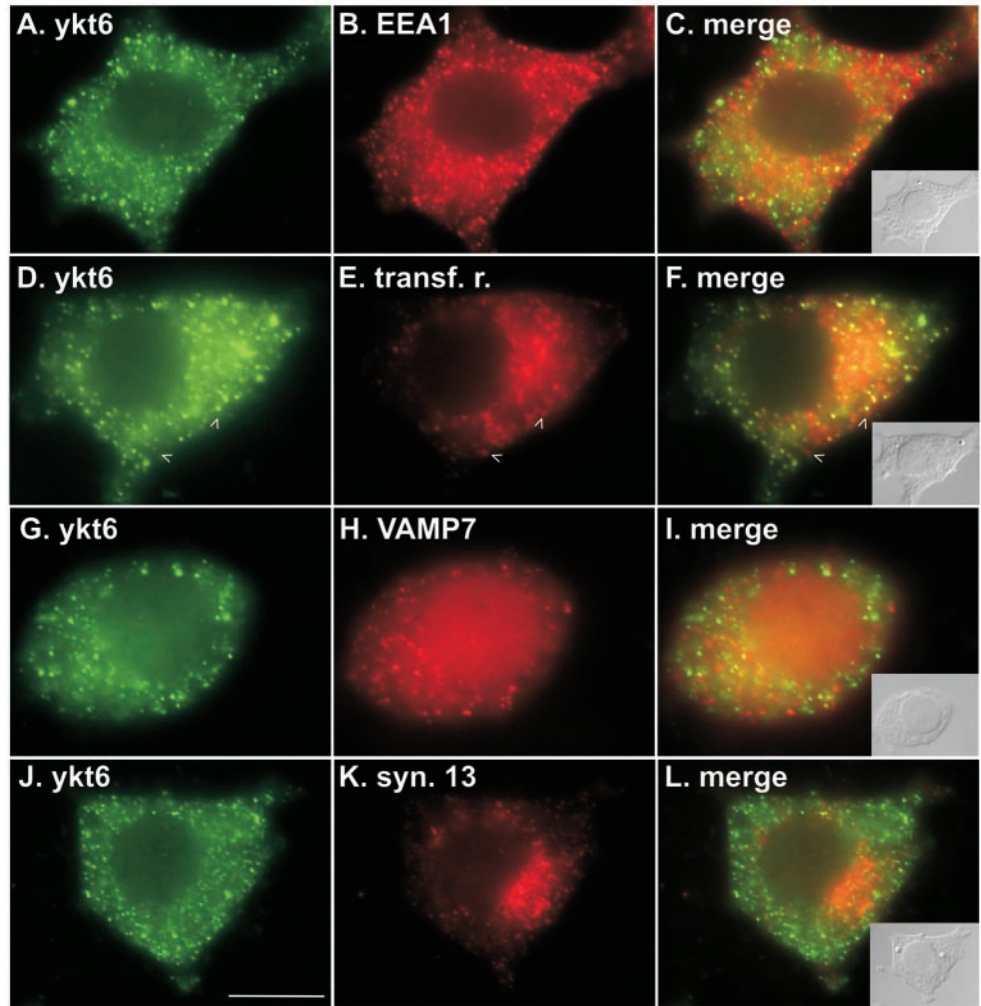
Figure 6. Ykt6-containing membranes do not overlap significantly with membranes of the endosomal pathway. PC12 cells were fixed and stained with anti-ykt6 antibodies and FITC-labeled secondary antibodies (A, D, G, and J) and costained with the following primary antibodies followed by Texas Red–labeled secondary antibodies: EEA1 (B), transferrin receptor (E), VAMP 7 (H), and syntaxin 13 (K). Green and red images from the same field and focal plane were merged (C, F, I, and L). Arrowheads in F demonstrate that individual red and green spots do not overlap, even though some yellow is visible in the perinuclear region of the cell. Insets show DIC images of the respective fields. Bar, 10 μm.

even though the colors overlapped in these cases, the apparent structures did not directly superimpose, leading to the conclusion that the yellow resulted from distinct overlapping structures. In the peripheries of the cells, the green and red spots did not overlap (Figure 6F, arrowheads). In neurons, VAMP 7 was reported to be present on a novel recycling compartment involved in neurite outgrowth (Coco et al., 1999). No colocalization of VAMP 7 was observed with ykt6-containing membranes (Figure 6, G–I). It has also been reported that the major AP-3–coated membranes in mammalian cells did not colocalize with secretory or endosomal markers (Simpson et al., 1997). Again, these membranes did not overlap significantly with ykt6 (unpublished data). Figure 6, J–L, demonstrates that syntaxin 13, a SNARE in early and recycling endosomes implicated in neurite extension in neurons (Hirling et al., 2000) and the recycling of plasma membrane proteins in PC12 cells (Prekeris et al., 1998), also did not significantly colocalize with ykt6 in PC12 cells.

We next considered markers of late endosomal and lysosomal compartments. Neither syntaxin 7 (Figure 7, A–C) nor VAMP 7 (Figure 6, G–I), both reported to be present in late endosomes (Wong et al., 1998; Advani et al., 1999; Coco et al.,

1999; Lafont et al., 1999; Prekeris et al., 1999; Mullock et al., 2000; Nakamura et al., 2000; Ward et al., 2000; Wade et al., 2001), overlapped with ykt6 significantly, though without costaining it would have been difficult to distinguish them. Although the cell in Figure 7, A–C, is a very mild example, the syntaxin 7 membranes tended to be denser than ykt6 in cytoplasm just under the plasma membrane, especially near emerging neurites (Figure 7C, arrowheads). Enlarged neurite terminals often contained both ykt6 and syntaxin 7 labeling but little or no overlap was observed (Figure 7C, detail). The lysosomal marker cathepsin D also did not generally overlap with ykt6 (Figure 7, D–F). However, as indicated by the arrows in Figure 7, G–L, there were a consistently small number of specific spots that coincided between these two markers. The number of overlapping spots was approximately the same or slightly less than that seen with synaptotagmin (Figure 5, J–N). Our interpretation is that, as with the synaptotagmin overlap, the two kinds of structures may have shared a common origin compartment or intermixed to a degree in their life cycle. However, the functional relationship must be limited because of the low number of overlapping spots, and to the fact that in ng108
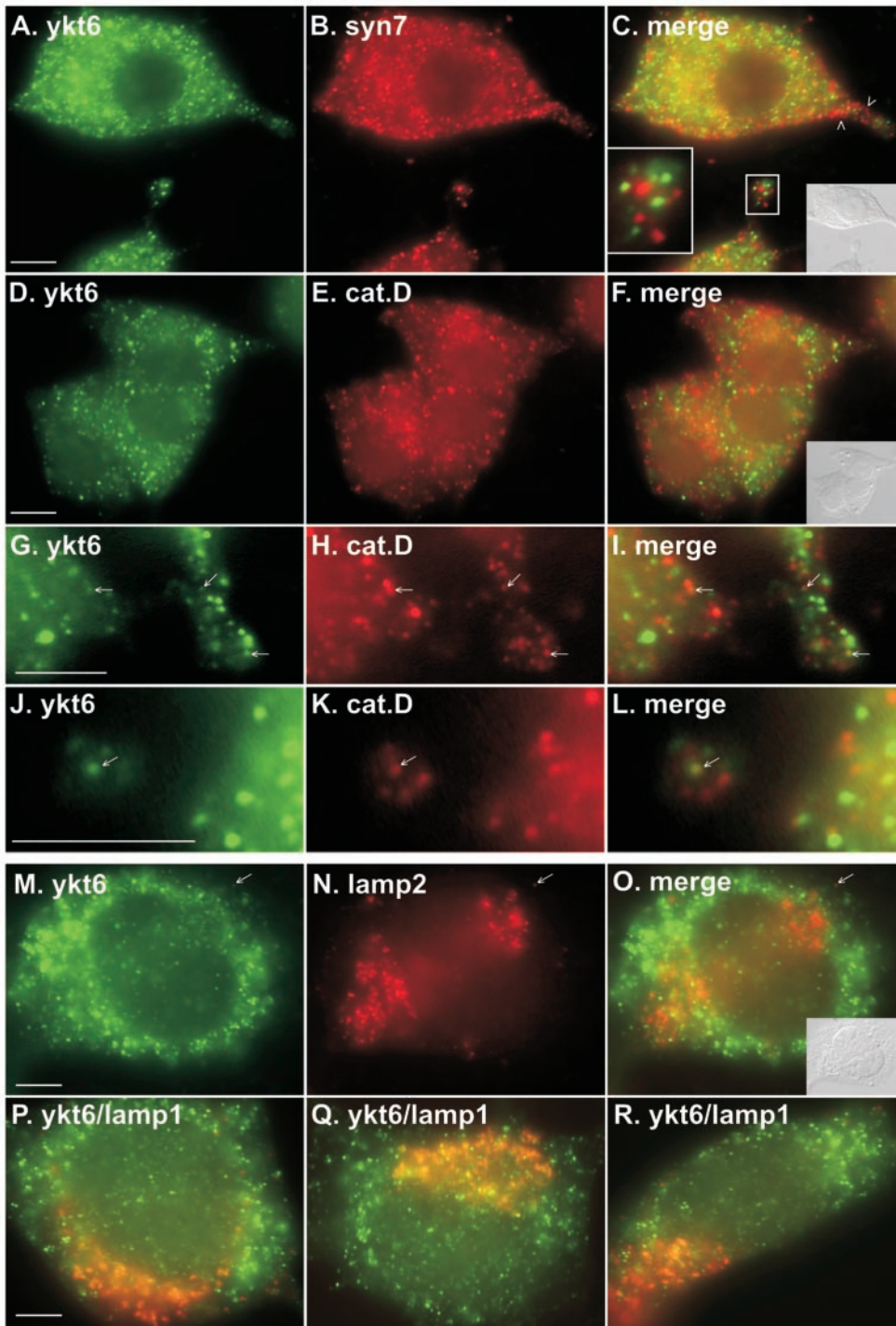
Figure 7. Ykt6-enriched membranes display a very limited overlap with lysosomal markers. PC12 cells (A–L) or ng108 cells (M–R) were fixed and stained with anti-ykt6 antibodies and FITC-labeled secondary antibodies (A, D, G, J, M, and P–R) and costained with syntaxin 7 (B), cathepsin D (E, H, and K), LAMP2 (N) or LAMP1 (P–R) followed by Texas Red–labeled secondary antibodies. Green and red images from the same field and focal plane were merged (C, F, I, L, O, and P–R). Arrowheads in C point to a region under plasma membrane near the base of a neurite that is more heavily stained with syntaxin 7 than ykt6. Arrows in G–O highlight a few structures that appeared to correspond between ykt6 and cathepsin D or LAMP2. As can be seen in merged whole-cell views (F, O, and P–R), these represent a very small proportion of the total spots. Insets show DIC images of their respective fields and a magnified neurite tip in C. Bars, 6.25 μm.

cells, even though occasional spots overlapped, ykt6 and lysosomal markers displayed very different overall distributions within the cells. For example, LAMP-1 and LAMP-2, which are known components of late endosomes and/or lysosomes (Chen *et al.*, 1985), were present on spotty structures that were densest in a juxtanuclear zone, presumably surrounding the Golgi, whereas ykt6 structures were more uniformly distributed throughout the cytoplasm (Figure 7, M–R). It is worth noting that the lack of ykt6 colocalization with any marker of the endosomal system did not appear to result from mere heterogeneity of these compartments; the ykt6 staining was far more distinct from any marker than,

for example, different late endosome/lysosome markers were distinct from each other. For example, cathepsin D and LAMP-1 in our hands overlapped extensively in ng108 cells (unpublished data).

Because none of our specific subcellular markers for secretory and endosomal compartments had overlapped significantly with ykt6 (Figures 5–7), we performed several further experiments to test for a more general association of ykt6 with secretory and endosomal compartments. In the first experiment, PC12 cells were transfected with GFP-tagged vesicular stomatitis virus (VSV) G protein ts045, a temperature-sensitive secretory membrane cargo protein that is retained in the ER at 39°C and undergoes synchronous movement through the constitutive secretory pathway upon temperature shift to 32°C (Scales *et al.*, 1997). As seen in Figure 8, A–I, GFP-G ts045 did not colocalize with ykt6-positive structures at any point in its movement to the plasma membrane. We examined the spotty post-Golgi secretory carriers carefully (Figure 9, G–I, and a 15-min timepoint; unpublished data) but never found significant overlap with ykt6, indicating that the ykt6 compartment does not lie along the default secretory pathway in these cells.

We also incubated cells at 15°C to block secretion at the VTC-to-Golgi stage and incubated PC12 cells with brefeldin A to disrupt trafficking through the Golgi. Although both of these treatments had pronounced effects on the VTC and Golgi markers, they had no noticeable effect on the distribution of the ykt6 compartment (unpublished data). In an experiment to test for association with the general endocytic pathway, we incubated PC12 cells with Texas Red–conjugated dextran (TR-dextran) for a 10-min pulse and then chased this bulk-phase endocytic marker through the endocytic system to lysosomes. TR-dextran colocalized well with EEA1 at early timepoints (Figure 8, J–L) and significantly with cathepsin D at later timepoints (Figure 8, M–O). On extensive incubation of PC12 cells with Texas Red-dextran to label all stages of the endocytic pathway, we were able to detect a small number of ykt6-containing spots that were positive for Texas Red-dextran (Figure 8, P–R). However, the colocalization was much less frequent than with the other markers. This is consistent with the finding that ykt6 exhibited a very minor overlap with cathepsin D (Figure 7. G–L). Once again, our interpretation is that the ykt6 compartment may be biosynthetically related to lysosomes and thus is accessible to a very minor degree to bulk phase endocytic markers. In summary, all of our experiments up to this point indicate that ykt6 is enriched in an unidentified, widely dispersed cytoplasmic organelle with a particular preponderance and/or relevance in neurons. Given the general properties of rat ykt6 as a SNARE, it is likely that ykt6 is important for the correct trafficking of membrane into or out of that compartment.

Relationship of the ykt6 Compartment to the Cytoskeleton

Because many cytoplasmic organelles maintain their steady state distributions through associations with the cytoskeleton, we tested whether the ykt6 compartment was colocalized with or dependent on the cytoskeleton. As seen in Figure 9, A–C, the ykt6 distribution and actin microfilaments visualized with Alexa Fluor 594-phalloidin looked dissimilar and did not visibly colocalize in PC12 cells. Most of the

filamentous actin was present in the juxtanuclear zone or in a ring just under the plasma membrane, unlike ykt6. Microtubules stained with an anti-tubulin antibody crisscrossed the cytoplasm and may have overlapped with ykt6 in a few instances, but it was difficult to judge whether there was a bona fide association (Figure 9, D–F). To test whether the ykt6 compartment was dependent on microtubules for its steady state distribution, we used the drug nocodazole to disassemble microtubules and examined the effects on several organelle markers including ykt6. Nocodazole did not visibly perturb the ykt6 distribution (Figure 9, I vs. L); however, early endosome EEA1 (Figure 9, G vs. J), recycling endosome transferrin receptor (Figure 9, H vs. K), and GM130 Golgi vesicles (unpublished data) translocated centrifugally, reflecting a role for microtubules in their distribution. In summary, we found no evidence of ykt6 compartment association with or dependence on actin microfilaments or nocodazole-dependent microtubules.

The Profilin-like Domain Is Necessary and Sufficient for the Specialized ykt6 Subcellular Localization

To investigate the structural determinants for ykt6 targeting to its unique compartment, we constructed a series of myc-ykt6 constructs for expression and localization in PC12 cells (see diagram in Figure 10A). We first investigated the role of protein prenylation in ykt6 localization by constructing two myc-ykt6 constructs, one in which the two C-terminal cysteines were mutated to alanine (myc-rykt6 CC194,195AA) and another in which the last five amino acids were removed (myc-rykt6ΔCCAIM). Surprisingly, when expressed in PC12 cells and stained with anti-myc antibodies, both constructs gave deconvolved staining patterns that appeared remarkably normal (Figure 10, E and F). The constructs seemed normally punctate, and no increase in diffuse cytosolic fluorescence was seen. To test whether these constructs were in fact membrane-associated, transfected cells were homogenized, the nuclei removed by centrifugation, and the postnuclear supernatants were centrifuged at $100,000 \times g$. The resulting supernatant was retained, and the pellet was rehomogenized in buffer and repelleted before analysis by SDS-PAGE and immunoblot. As seen in Figure 10C, both mutant constructs maintained a significant presence in the washed membrane pellets. Although less was present in the pellets than for the wild-type myc-rykt6 construct, this might be expected for a solely protein-interaction–mediated membrane association without the prenyl groups to embed in the bilayer. Importantly, much more membrane association was observed for these constructs than for truly cytosolic components like GFP. We confirmed that these C-terminal mutants were in fact not prenylated using a detergent partitioning experiment similar to that in Figure 2. As can be seen in Figure 10D, wild-type myc-rykt6 partitioned significantly into the detergent phase of a Triton X-114 suspension, indicative of extreme hydrophobicity. On the other hand, the C-terminal mutants partitioned primarily into the aqueous phase, indicative of the loss of a major hydrophobic determinant, i.e., one or two C-15 prenyl group(s). It was apparent that the wild-type myc-rykt6 construct partitioning into the detergent phase was less complete than for endogenous PC12 ykt6 (Figure 10D). We believe that overexpression of this construct saturated the prenylation machinery, resulting in only partial prenylation.
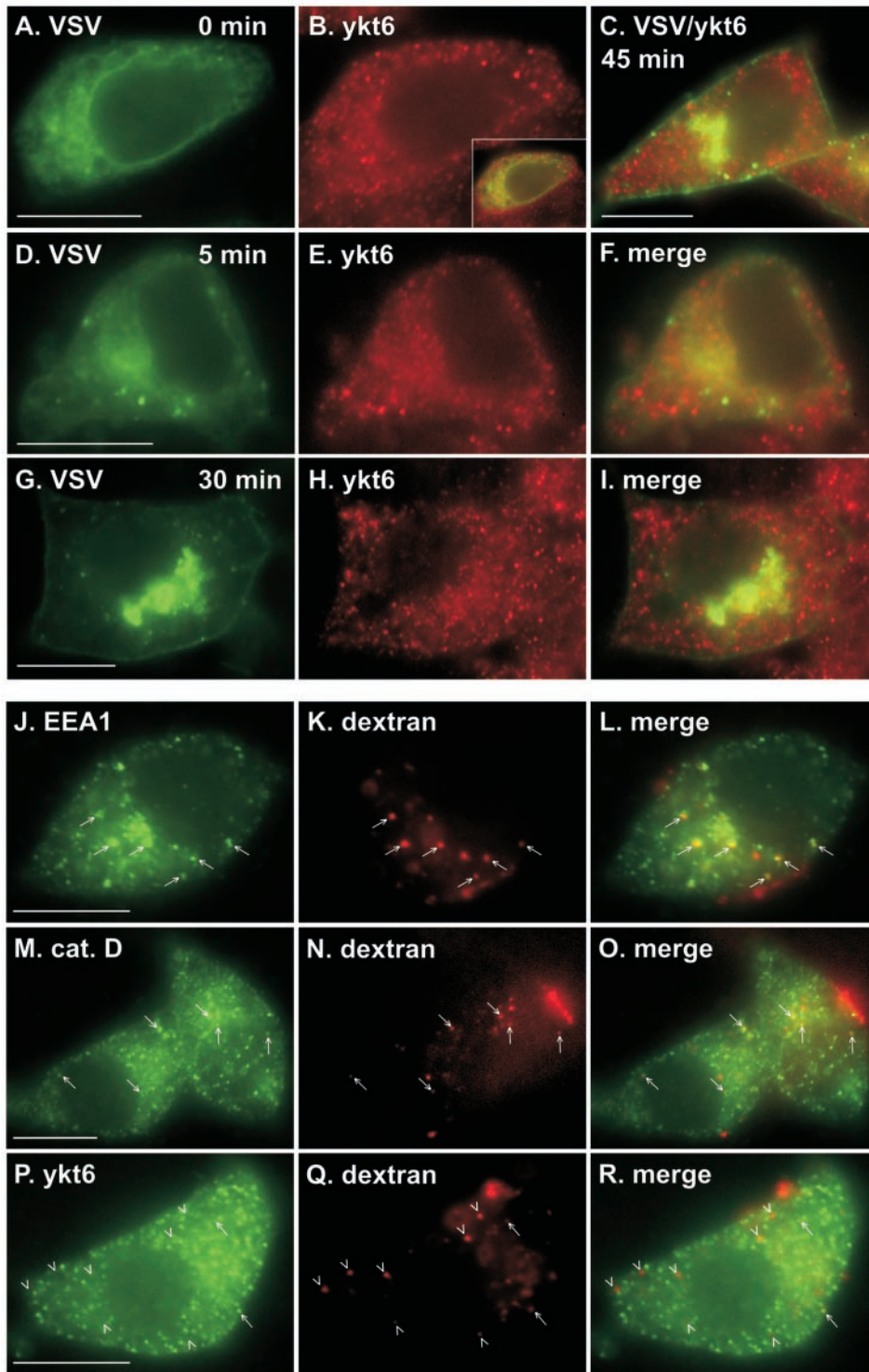
Figure 8. Possible association of ykt6 with the constitutive endocytic pathway, but not the constitutive secretory pathway. (A–I) PC12 cells were transfected with VSV G-GFP (ts045 strain) and held at 40°C overnight to accumulate the construct in the ER. Cells were then fixed directly (A and B) or incubated for the indicated chase times at 32°C before fixation (C–I). After fixation, cells were stained with anti-ykt6 antisera and Texas Red–labeled secondary antibodies. (A and B) ykt6- and VSV-GFP-images of the same field at 0 min, whereas C shows a merged image at 45 min. (F and I) Merged images, at the indicated chase times, of the two fields preceding them. Inset in B is a merge of A and B. (J–R) PC12 cells were incubated with Texas Red–labeled dextran for 10 min (J–O) or 170 min (P–R) and chased in dextran-free medium for 0 min (J–L, P–R) or 80 min (M–O). After fixation, cells were stained with anti-EEA1 (J–L), anti-cathepsin D (M–O), or anti-ykt6 (P–R) antisera and FITC-labeled secondary antibodies. Arrows point out the many stained structures that overlapped dextran for EEA1 and cathepsin D and a few that overlapped for ykt6. Arrowheads point out that the large majority of Texas Red–positive structures did not overlap with ykt6. Bars, 10 μm.

In support of this explanation, the endogenous ykt6 present in the overexpressing cells also partitioned less completely into the detergent phase (unpublished data).

Because protein prenylation was not required for membrane association and ykt6 localization, we had an excellent opportunity to determine protein domains responsible for these activities. As shown in Figure 10G, deletion of the entire N-terminal domain, residues 1–136 (myc-rykt6ΔNT), resulted in a dramatic loss of specific localization. In fact, this construct appeared to simply traverse the default secre-
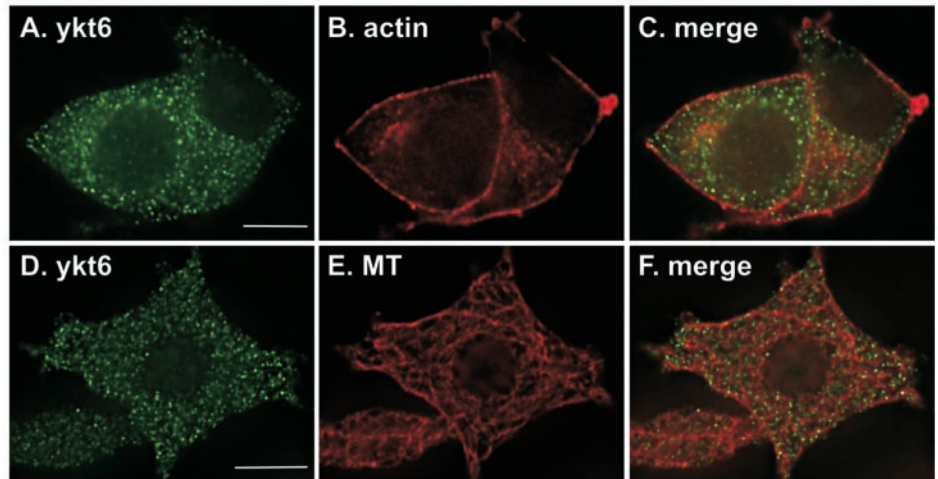
Figure 9. Ykt6 distribution does not appear to involve actin filaments or nocodazole-sensitive microtubules. (A–F) PC12 cells were fixed and stained with anti-ykt6 (A and D), Alexa Fluor 594-phalloidin (B), or anti–α-tubulin (E). Green and red images from the same fields were merged (C and F). (A–F) Deconvolved single optical sections. (G–L) PC12 cells were either fixed and stained as normal (G–I) or incubated with 30 μM nocodazole for 2 h and then fixed and stained (J–L). Coverslips were stained with anti-tubulin (G–L), anti-ykt6 (I and L), anti-EEA1 (G and J), or anti-transferrin receptor (H and K) antisera. The indicated staining is shown for each panel, with the anti-tubulin pattern for the same field shown in the inset. Bars, 10 μm.
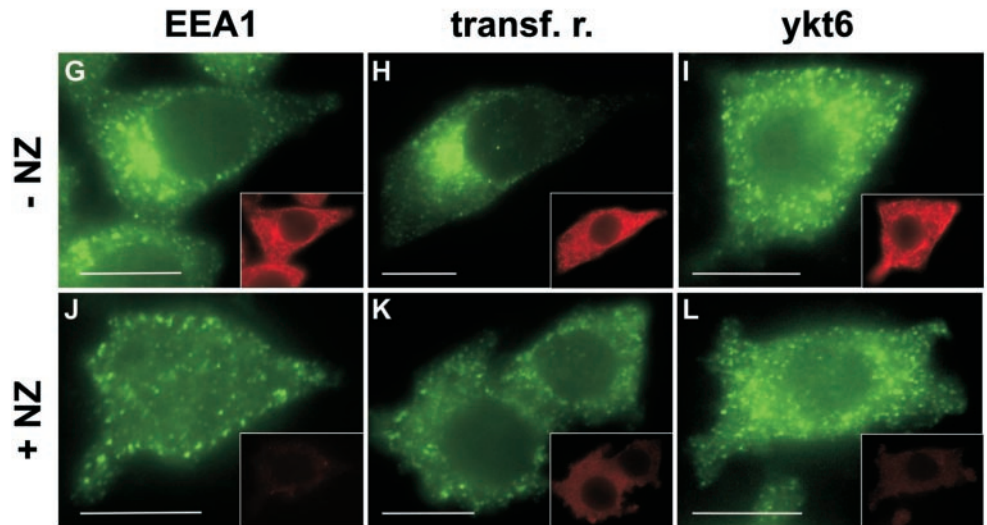
tory pathway and was clearly visible in the Golgi (see Golgi overlay, inset) and the plasma membrane. Hence, the ykt6 NT domain was necessary for proper localization. To test whether this was merely a result of an abnormally truncated SNARE as opposed to a specific requirement for the ykt6 NT, we created a hybrid construct, myc-rykt6(sec22b-NT), containing the structurally related profilin-like NT domain from mouse sec22b, an ER and VTC SNARE, and the SNARE motif and prenylation motif of ykt6. As shown in Figure 10H, this construct behaved indistinguishably from myc-rykt6ΔNT, establishing that not only is the ykt6 NT domain necessary for proper targeting, but it is a specific property of ykt6-NT and cannot be mediated by other profilin-like SNARE NT domains. Finally, we expressed a construct containing only the ykt6 NT domain, myc-rykt6-NT, and examined its localization using anti-myc antibodies. As seen in Figure 10I, the ykt6 NT domain was capable of generating a characteristic spotty dispersed localization, even in the absence of the SNARE motif or protein prenylation. The degree of overlap in these cells between anti-myc and anti-ykt6 staining was at least 50% (unpublished data),

as it was for cells transfected with full-length myc-ykt6 (see Figure 4). However, it is not formally possible to determine from this experiment whether myc-ykt6 NT and endogenous ykt6 colocalize. To test whether the ykt6 NT domain precisely targeted to the bona fide ykt6 compartment containing endogenous ykt6, we expressed myc-tagged yeast Ykt6p, which shares 48% sequence identity with rat ykt6, in PC12 cells, and costained with anti-myc and anti-rat ykt6 antibodies. We found that, as expected, chicken anti-rat ykt6 antibodies did not recognize the yeast protein, as evidenced by a lack of increased staining of cells that were clearly overexpressing and brightly stained with anti-myc (unpublished data). As shown in the deconvolved images in Figure 10, J–L, the yeast construct, myc-yYkt6p, overlapped significantly with endogenous rat ykt6 in transfected PC12 cells, demonstrating that the structural determinants for specific ykt6 targeting are conserved in the two species. Finally, as illustrated in the deconvolved images of Figure 10, M–O, the yeast Ykt6p NT domain on its own (myc-yYkt6p-NT), was able to colocalize with endogenous rat ykt6 on the specialized compartment. In summary, the experiments of Figure
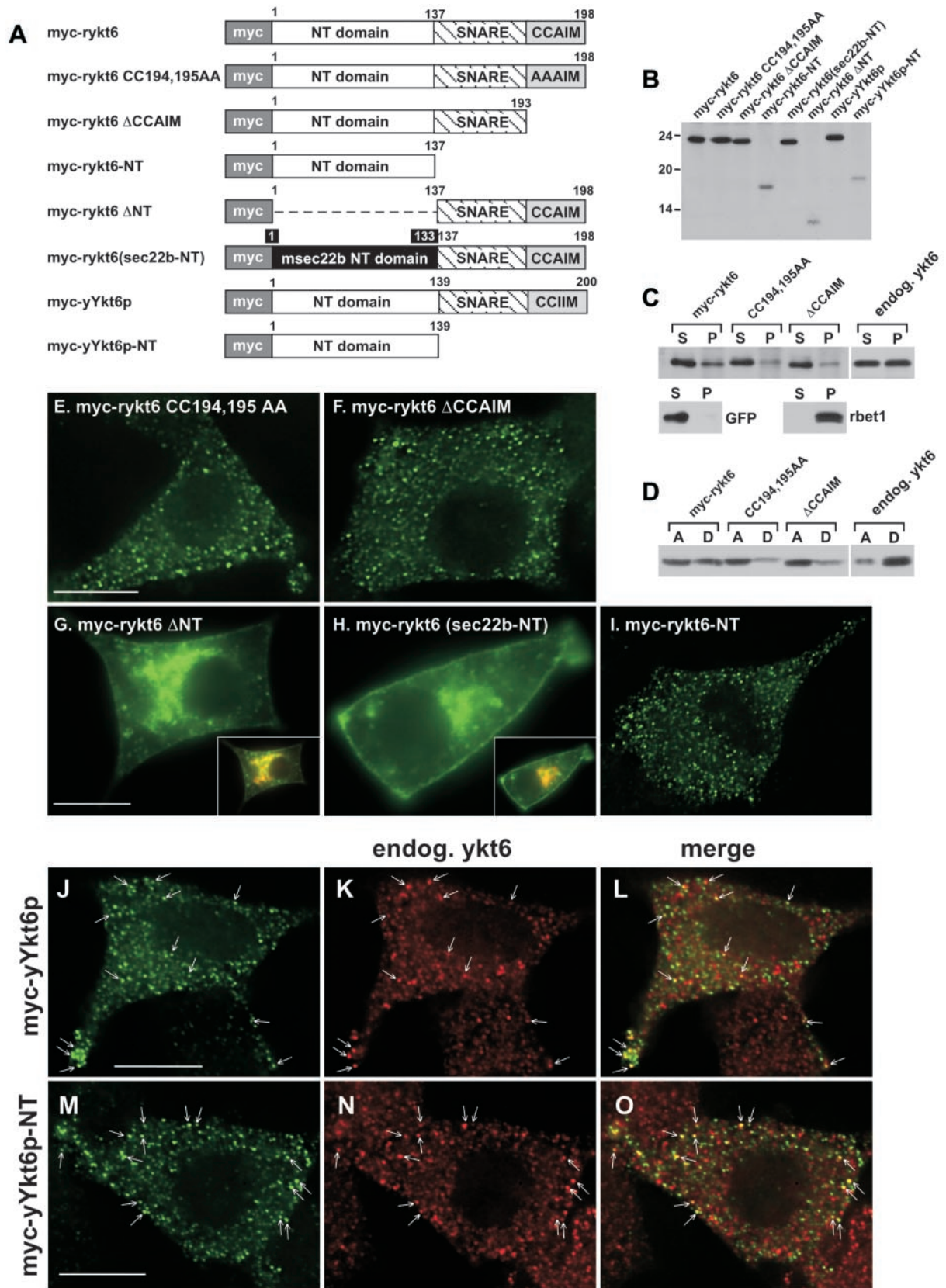
10 demonstrate that although protein prenylation contributes to tighter membrane association, the ykt6 NT domain is both necessary and fully sufficient for targeting to the specialized ykt6 vesicular structures. Furthermore, the structural determinants for this targeting are shared by mammalian and yeast ykt6, but not by other SNAREs containing profilin-like NT domains.

Rat ykt6 Is Present on Membranes with a Buoyant Density Similar to Lysosomes

To extend the intracellular localization studies, we examined the membrane-bound ykt6 by subcellular fractionation on equilibrium iodixanol gradients. Postnuclear supernatants were prepared from PC12 cells and the membranes were separated from cytosol by centrifugation through a density barrier and collected on a pad of dense iodixanol (see MATERIALS AND METHODS). The membranes were then layered under a 5–25% linear gradient of iodixanol and centrifuged to equilibrium. As evident in Figure 11, ykt6-enriched membranes floated in these gradients to a peak at 16% iodixanol in fractions 7 and 8. There was also some ykt6 at the bottom of the gradient and trailing up toward the peak in fractions 7 and 8. This may have been loosely membrane-associated ykt6 that dissociated before or during the experiment. In similar gradients on mouse and rat brain postnuclear membranes, a much higher proportion of the ykt6 floated, and almost none remained at the bottom of the gradient (unpublished data). Importantly, the floatation of most of the ykt6 demonstrates that the punctate ykt6-containing structures observed in Figures 5–10 are likely a membranous organelle rather than, for example, cytosolic protein aggregates. The density of the ykt6-containing membranes was lighter than that of Golgi, as marked by p115, but denser than early endosomal membranes marked by EEA1 (Figure 11A). Ykt6 membranes were also less dense than the dense, presumably TGN membranes containing syntaxin 6. Syn-

Figure 11. Fractionated ykt6-enriched membranes have a buoyant density similar to lysosomes. PC12 cells were homogenized and postnuclear membranes were isolated and loaded at the bottom of a continuous 5–25% iodixanol gradient. After centrifugation to equilibrium at 150,000 × g, the gradient was unloaded from the bottom, and individual fractions were analyzed by SDS-PAGE and immunoblotting with the antibodies indicated in the legend above. Percent iodixanol was determined with a refractometer. Panels A–C are from the same gradient. Similar results were obtained in other gradients.

Figure 10 (facing page). The ykt6 NT domain is necessary and sufficient for targeting to the ykt6 compartment. (A) Diagram of myc ykt6 constructs used in this study. yYkt6p refers to the yeast homolog and rykt6 refers to rat ykt6. (B) Immunoblot of PC12 cell lysates expressing the constructs used in this study. (C) Membrane association of myc-rykt6, myc-rykt6 CC194,195AA, and myc-rykt6ΔCCAIM in transfected PC12 cells. Shown are immunoblots of soluble supernatants (S) from a 100,000 × g centrifugation of postnuclear supernatant and the washed, insoluble membrane pellets (P). GFP was expressed as a control largely cytosolic protein, whereas rbet1 illustrates the behavior of an integral membrane protein in the same sample. (D) Partitioning of cytosolic myc-ykt6 constructs between aqueous (A) and detergent (D) phases of a Triton X-114 separation. Endogenous PC12 cell cytosolic ykt6 in nontransfected cells is shown for comparison. (E–I) Localization of the indicated rat myc-ykt6 constructs in transfected PC12 cells determined by anti-myc staining and FITC-labeled secondary antibodies. G and H were costained with anti-GM130, and the ykt6/GM130 merge for the displayed fields are shown in insets. E, F, and I are deconvolved single optical sections. (J–O) Single deconvolved optical sections showing colocalization of yeast myc-ykt6 constructs and endogenous PC12 cell ykt6. PC12 cells were transfected with the indicated constructs and stained with anti-myc (J and M) and anti-ykt6 (K and N) antibodies. Green and red images from the same fields were merged (L and O). Bars, 10 μm.
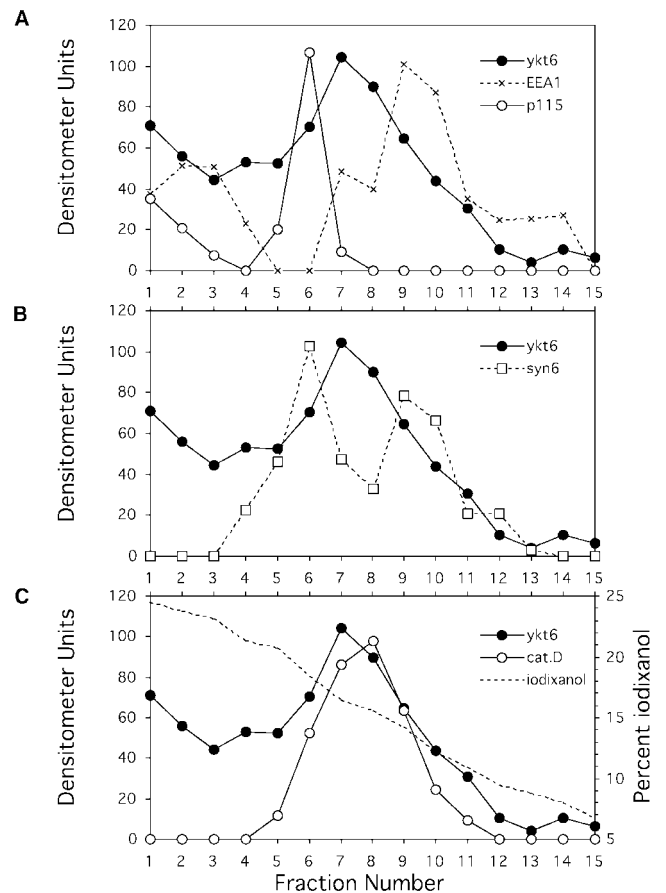
taxin 6 is localized to both TGN as well as endosomes (Bock et al., 1997; Simonsen et al., 1999) and often displayed a biphasic distribution on these gradients (Figure 11B). The denser peak, in fraction 6, overlaps with p115 and presumably represents TGN-localized syntaxin 6, whereas the lighter peak, in fractions 9 and 10, overlaps with the peak of EEA1 and presumably corresponds to endosomal membranes. The ykt6 peak is situated between the two peaks of syntaxin 6. Thus, ykt6 membranes are lighter than Golgi but slightly more dense than endosomes. The marker that most closely resembled the distribution of ykt6 membranes on the gradients was cathepsin D, which also peaked in fractions 7 and 8 (Figure 11C). The equilibrium fractionation experiments confirm that ykt6 membranes do not colocalize with Golgi as previously reported and suggest that the ykt6 compartment has a buoyant density similar to lysosomes.

In the Brain, ykt6 Is Expressed Predominantly in Neurons

Because ykt6 is expressed at high levels only in brain, it seems possible that the protein may play a specialized role in neuronal membrane transport. To test whether the ykt6 distribution within brain is consistent with a neuronal function, we immunolabeled rat brain sections with chicken anti-ykt6 antibodies and examined the samples using bright-field light microscopy. Ykt6 was expressed widely in the brain, e.g., in the cerebral cortex, the hippocampus, and the striatum (unpublished data), with the most strongly stained cells being present in the cortex. In both the hippocampus and the cerebral cortex (see Figure 12), most stained cells were pyramidal cells. Staining was strong throughout the cytoplasm of the cell bodies and large dendrites. Some smaller, nonpyramidal-shaped neurons, most likely inter-neurons, were also clearly stained. The neuropil areas between the cell bodies (containing a meshwork of axons, boutons, dendrites, spines, glial cells, and processes) were very weakly labeled, though not totally immunonegative when compared with negative control sections (no primary antibody; unpublished data). Weak to moderate immuno-staining was seen in some glial cell bodies, e.g., in the hippocampal stratum radiatum and in the corpus callosum, but no staining was present around blood vessels (where astrocytic processes are typically found). Though we did not discern specific immunolabeling of synaptic structures (axon terminals, spines), we cannot exclude the presence and function of ykt6 in these structures. The protein may well be present in these structures at a lower level. Also, because the size, or thickness, of these structures is low compared with that of the cell bodies, the surface labeling of the sections may appear weaker. We do not find any indications, however, that ykt6 is specifically concentrated in axons or axon terminals. Also note that the staining technique used, which involves significant cytoplasmic spreading of the chromophore, did not provide sufficient resolution to make out subcellular structures such as tubulovesicular membranes. Taken together, the results in brain sections indicate that ykt6 is specifically enriched in brain neurons, implying a specialized role in neuronal function.

Rat ykt6 Exhibits R-SNARE Assembly Properties in SNARE Complexes

We wanted to establish whether rat ykt6 could assemble into SNARE complexes, and if so, what its assembly properties would be. It is well known that SNAREs from various transport steps can assemble promiscuously in solution to form noncognate SNARE complexes (Fasshauer *et al.*, 1999; Yang *et al.*, 1999). Despite this level of nonspecificity in vitro, SNAREs maintain a rather strict conservation of the four structural positions within a complex (Antonin *et al.*, 2002). Each t-SNARE complex seems to involve three Q-SNAREs, which may preassemble together to serve as the binding site for a fourth, R-SNARE (often referred to as a v-SNARE). Rat ykt6, because of its zero-layer arginine, would be predicted to bind to t-SNARE complexes containing three Q-SNAREs. An ER/Golgi quaternary complex consisting of three Q-SNAREs, syntaxin 5, membrin, and rbet1, and one R-SNARE, sec22b, can be formed in solution and detected by gel filtration (Xu *et al.*, 2000). We examined the assembly
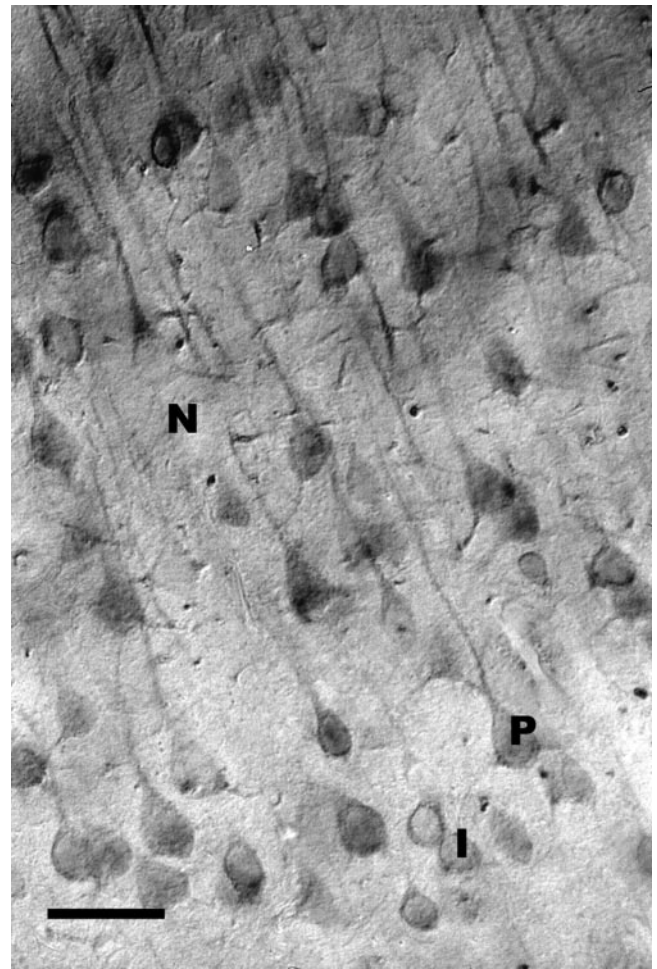

Figure 12. Brain ykt6 is expressed selectively in neurons. Vibratome section of rat brain (cerebral cortex) immunolabeled for ykt6. Note moderately to strongly labeled cell bodies, most of which are pyramidal cells (P). Strong labeling is also seen in apical and basal dendrites. Weak to moderate staining is present in the neuropil (N) between cells. Some immunopositive cells are smaller and rounder, probably representing interneurons (I). No immunopositive glial cell profiles are evident in this field. Scale bar, 50 μm.

properties of rat ykt6 by testing whether it would form a quaternary complex or alternatively any subcomplexes, with any combination of three of the ER/Golgi SNAREs. As shown in Figure 13, top panel, ykt6 was incorporated into a high-molecular-weight complex with syntaxin 5, membrin, and rbet1. This complex was likely a quaternary complex, because no high-molecular-weight ykt6 was observed with any subset of those three Q-SNAREs. This behavior mimics exactly the assembly properties of sec22b, which also binds only to the combination of syntaxin 5, membrin, and rbet1 but no subset of them (Xu *et al.*, 2000). Also note that no potential complexes containing both ykt6 and sec22b are evident, consistent with the idea that both proteins play the same structural role and therefore cannot coexist in the same complex. This is not merely a trivial result of both proteins containing the arginine, per se, because mutant SNAP-25
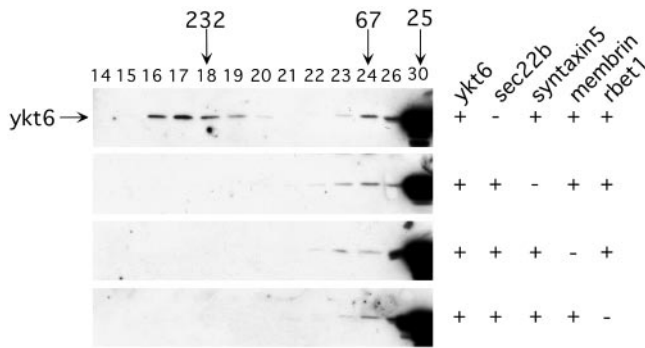
Figure 13. Rat ykt6 assembles with other SNAREs similarly to the R-SNARE sec22b. Purified bacterially expressed soluble ytkt6 was mixed with sec22b, syntaxin 5, membrin, and rbet1 in the indicated combinations of proteins. After an overnight incubation at 4°C, the proteins were gel-filtered on Superdex 200, and individual column fractions were immunoblotted with anti-ykt6. Note that rat ykt6 does not bind significantly to any subset of the ER/Golgi Q-SNAREs; it does, however, incorporate into a quaternary complex containing all of them (fractions 16–18, top panel). Elution positions of size calibration proteins are indicated with arrows above the fraction numbers.

containing arginine at either or both of its zero layer positions can assemble with VAMP and syntaxin 1A to form a perfectly stable (though likely nonfunctional) complex in vitro (Scales *et al.*, 2001). In sum, Figure 13 indicates that rat ykt6 behaves structurally as a VAMP- or sec22b-like R-SNARE in its in vitro assembly patterns with other SNAREs. Note that just because ykt6 can assemble with ER/Golgi SNAREs to form complexes does not mean that ykt6 normally functions in ER/Golgi transport. However, it is consistent with the possibility that at the transport step where ykt6 *does* function, it does so by binding to a complex of three Q-SNARE helices on an opposing membrane.

Cytosolic Rat ykt6 Is Not Reactive Toward Noncognate SNAREs

Because purified recombinant ykt6 could enter noncognate SNARE complexes with ER/Golgi SNAREs (Figure 13) and considering that soluble v-SNAREs can be potent inhibitors of membrane fusion (Weber *et al.*, 1998; Scales *et al.*, 2000; Brickner *et al.*, 2001), we wondered how the cytosolic pool of ykt6 avoids interfering with and inhibiting its own or other transport steps in vivo. One possibility is that cytosolic ykt6 is conformationally regulated such that its SNARE motif is not reactive toward other SNAREs. We tested this possibility by partially purifying ykt6 from rat brain cytosol and testing it in similar noncognate SNARE complex reactions to those in Figure 13. As shown in the silver-stained gel in Figure 14A, after several chromatography steps we obtained a simplified pattern of protein bands among which ykt6 was visible, although not abundant. The partial purification included a gel filtration step that removed high-molecular weight factors such as NSF. When the partially purified cytosolic ykt6 or a comparable amount of the recombinant purified ykt6 were tested for SNARE complex formation as in the previous experiment, the recombinant, but not the
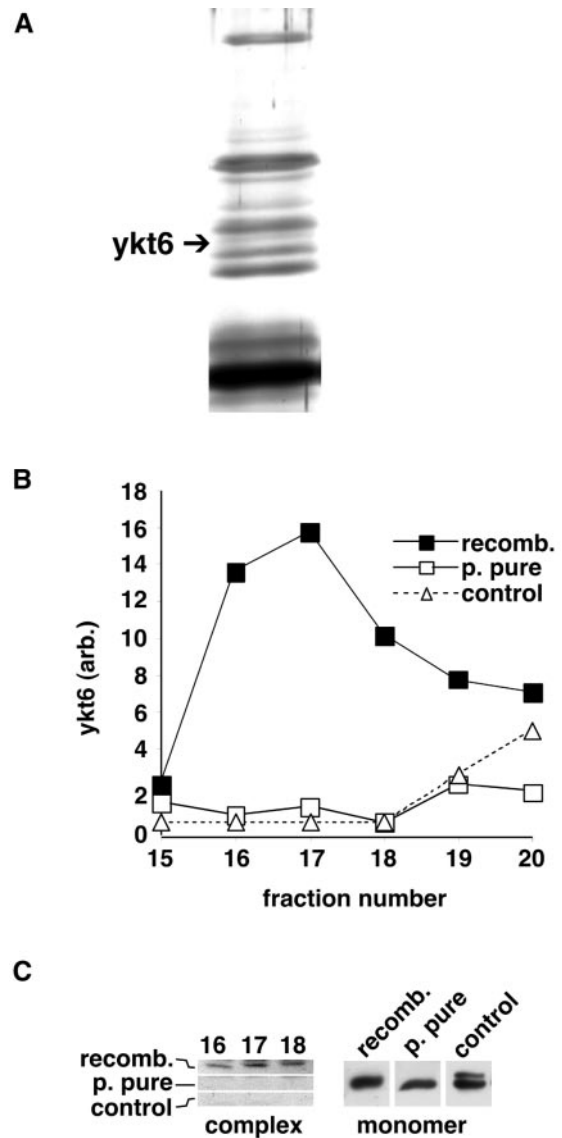

Figure 14. Partially purified cytosolic ykt6 is not activated for SNARE complex formation. (A) Silver-stained SDS-PAGE of cytosolic ykt6 partially purified as described in MATERIALS AND METHODS. Identity of the ykt6 band indicated by an arrow was determined by immunoblotting (unpublished data). (B) Partially purified cytosolic ykt6 or an equal amount of fully purified recombinant ykt6 were mixed with purified recombinant syntaxin 5, membrin, and rbet1, exactly as in Figure 13, except that the ykt6 fractions were more dilute. After an overnight incubation on ice, the reactions were gel filtered as in Figure 13, and column fractions were acetone precipitated, immunoblotted with anti-ykt6 antibodies, and quantified. "Control" refers to a reaction containing recombinant ykt6 but no other SNAREs. (C) Left panel: immunoblots of the indicated column fractions that were quantified for part B. Right panel: the monomer peak fraction from each gel filtration reaction was immunoblotted to demonstrate that equivalent total amounts of ykt6 were recovered from the column (unbound ykt6 migrated similarly for both preparations). Left and right panels were taken from different exposures of the immunoblot, because the monomer fractions were overexposed when complex fractions were properly exposed. Equivalent results were obtained in several experiments.
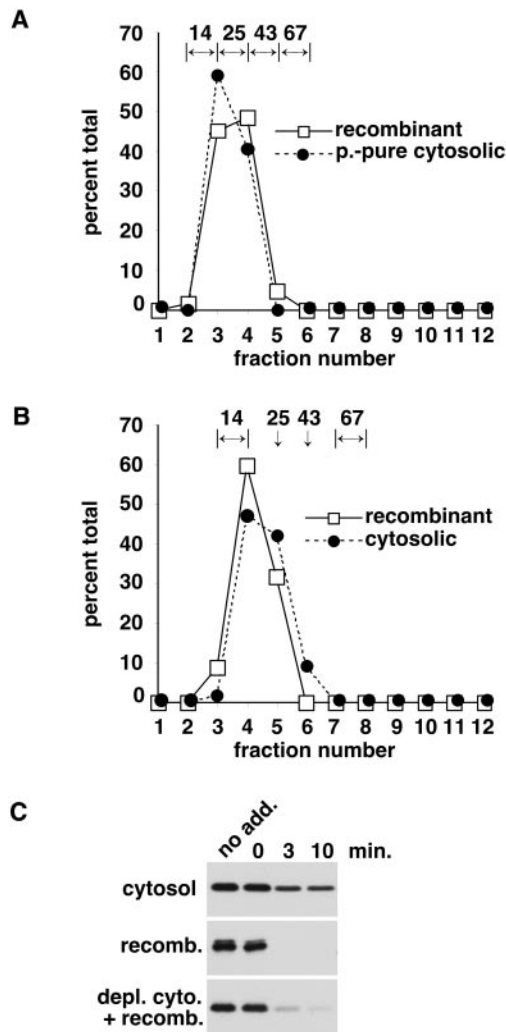
Figure 15. Cytosolic ykt6 is not present in a tight protein complex but is inherently more protease resistant than recombinant ykt6. (A) Partially purified cytosolic ykt6 (see Figure 14) or purified recombinant ykt6 were sedimented for 20 h on 5–30% glycerol velocity gradients. Fractions were unloaded from the top and immunoblotted with anti-ykt6 antisera, and the amount of ykt6 present was quantitated and plotted. Positions of marker proteins ribonuclease (14 kDa), chymotrypsinogen A (25 kDa), ovalbumin (45 kDa), and albumin (66 kDa), run in a separate gradient in the same experiment, are indicated above. When the marker protein fell approximately equally in two consecutive fractions, a bracket indicates the range. When there was a single major fraction, a vertical arrow denotes the peak. (B) Similar experiment to that in A except that crude rat brain cytosol, rather than partially purified cytosol, was fractionated for comparison to recombinant ykt6, and the gradient was run for 30 h. (C) Cytosol was either depleted (~90%) or mock-depleted of soluble ykt6 with anti-ykt6 antibody and protein A-Sepharose (see MATERIALS AND METHODS). The "missing" ykt6 in the depleted cytosol was then restored using purified recombinant ykt6. Another fraction of purified recombinant ykt6 was prepared by dilution in 5 mg/ml BSA. The mock-depleted cytosol ("cytosol"), the BSA-diluted recombinant ykt6 ("recomb."), and the depleted/restored cytosol ("depl. cyto. + recomb.") were incubated with protease K for the indicated times and then immunoblotted using chicken anti-ykt6 antibodies. Reactions labeled "no add." lacked protease.

cytosolic, ykt6 detectably entered SNARE complexes (Figure 14, B and C). The percent incorporation of ykt6 was very low using this low a concentration of ykt6; however, in repeated attempts the recombinant but never the cytosolic ykt6 was reactive at the same concentrations. Similar experiments demonstrated that ykt6 in crude, unpurified cytosol was also inactive in SNARE assembly reactions (unpublished data). Furthermore, this seemed to be due to inactivity of ykt6, as opposed to the presence of a general SNARE complex inhibitor in cytosol, because recombinant ykt6 maintained much greater activity even when mixed with crude cytosol (unpublished data). These experiments provide preliminary evidence for negative regulation of the cytosolic ykt6 SNARE motif.

Cytosolic ykt6 Is Not Present in a Tight Protein Complex

Speculative explanations for the nonreactivity of cytosolic ykt6 include the possibility that in the cytosol, ykt6 is tightly bound by another protein that sequesters the SNARE motif. This situation could also explain how cytosolic ykt6 remains soluble despite the hydrophobic prenyl modification (see Figure 2B), much as cytosolic prenylated rab is kept soluble by rab escort protein and GDI (Gelb *et al.*, 1998; Alory and Balch, 2001). Another possibility would be that the cytosolic ykt6 protein itself is inherently conformationally inactive, perhaps because of regulation by its own NT domain, prenyl moieties, or transiently associated regulatory proteins. To distinguish these two possibilities, we size-fractionated the partially purified cytosolic ykt6, recombinant ykt6, and crude cytosol to determine the native mass of ykt6. Although gel filtration is useful for separating a bound from unbound pool of a protein, as in Figures 13 and 14, it cannot be used for an accurate measure of molecular weight when a hydrophobic posttranslational modification such as prenylation is present, because this can artifactually retard migration. Velocity sedimentation, on the other hand, can be used to directly compare hydrophilic and hydrophobic proteins. As shown in Figure 15A, recombinant and partially purified cytosolic ykt6 precisely cosedimented at a rate consistent with a protein mass of, or just under, 25 kDa, the expected mass of monomeric ykt6. Likewise, recombinant ykt6 and ykt6 present in crude cytosol also closely cofractionated (Figure 15B), although ykt6 in cytosol may have sedimented slightly faster, a relative shift of at most a few kilodaltons. These sedimentations are inconsistent with the "escort protein" explanation for ykt6 solubility and nonreactivity toward noncognate SNAREs and therefore favor the hypothesis that cytosolic ykt6 itself is intrinsically inactive in SNARE assembly reactions.

Cytosolic ykt6 and Recombinant ykt6 Display Distinct Protein Conformations

To test whether a conformational difference between recombinant and cytosolic ykt6 was detectable, potentially explaining the nonreactivity of the latter, we tested crude cytosolic ykt6 and purified recombinant ykt6 for protease sensitivity using protease K. As shown in Figure 15C, cytosolic ykt6 was significantly more protease resistant, implying a significant conformational difference. Importantly, protease resistance was not readily transferable to

recombinant ykt6 upon addition to cytosol that had been depleted of endogenous ykt6. These results document an intrinsic conformational difference between recombinant and cytosolic ykt6—a difference that likely explains their different reactivities in SNARE assemblies. Because cytosol did not readily impart protease resistance to exogenous recombinant ykt6, the conformational difference could be the result of long-term regulation by a relatively irreversible posttranslational modification, for example, protein prenylation.

DISCUSSION

Our results documented several unanticipated features of rat ykt6. First, although yeast Ykt6p is involved in constitutive biosynthetic transport steps like ER-to-Golgi and Golgi-to-vacuole transport, mammalian ykt6 is expressed at high levels only in brain (Figure 3). Furthermore, within the brain, ykt6 was concentrated specifically in neurons (Figure 12). This strongly suggests that ykt6 has a specialized function in neurons, although we cannot rule out the possibility that it plays a fundamental, constitutive role in neurons but is functionally redundant with other SNAREs in tissues where little or no ykt6 is expressed, for example, liver. Second, rat ykt6, although significantly membrane-associated, is not localized to any of the well-characterized compartments of the secretory or endosomal systems (Figures 5–8). Together these findings make it very likely that ykt6 is present on vesicular membranes that are specialized for a trafficking pathway with particular significance to neurons. Determination of the function of this pathway in neurons will involve the physical isolation of ykt6-associated membranes and molecular identification of cargo molecules. This approach is likely to be more successful than continued subcellular colocalization studies using preconceived markers. Third, the amino-terminal profilin-like domain, and not the prenyl group(s), is the primary determinant for ykt6 binding to its specialized compartment. Although several SNAREs, including sec22 isoforms (yeast Sec22p and mammalian sec22a, sec22b, and sec22c), as well as VAMP 7, have structurally similar domains, targeting to the ykt6 compartment is not a general function of these domains and appears to be specific for the ykt6 NT domain. Although a mild effect of the NT domain on recombinant yeast Ykt6p SNARE complex formation has been reported (Tochio et al., 2001), ours is the first clearcut report of a specific function for a profilin-like NT domain on any SNARE. Fourth, cytosolic ykt6 appears to be negatively regulated so that its SNARE motif is not available for SNARE complex formation. Although the precise mechanistic basis of this phenomenon is not known, it does not appear to be mediated by tight binding with another cytosolic protein but instead may be a long-lasting conformational state. If so, this is an important form of SNARE regulation because an active, promiscuous cytosolic v-SNARE could be deleterious to its own and other transport steps.

Our results do not agree well with a previous study that analyzed ykt6 on rat liver membranes and found a colocalization of ykt6 with Golgi markers in NRK cells (Zhang and Hong, 2001). The differences are not likely due to isoform heterogeneity of ykt6; there is no evidence for multiple mammalian ykt6 genes or splicing isoforms, and the cDNA we used to generate antibodies only differed from that of Zhang et al. at four nonclustered amino acid residues. One possible explanation for the discrepancy in ykt6 intracellular localization is that different antibodies to ykt6 may recognize different pools of ykt6 in the cell. If ykt6 is rapidly cycling between two membrane stations, as are many SNAREs, it is possible that its conformation or binding partners precludes recognition in one or the other location. Thus, it is possible that ykt6 is cycling between the Golgi and the punctate ykt6 structures we observed but that our antibody recognized it only in the punctate structures. If this were the case, then the anti-myc antibody must have also recognized ykt6 in an identical, location-selective manner (Figure 4). Another potential reason for the discrepancy could be differences in ykt6 localization in different cell types. It is possible that ykt6 has different functions in kidney, where it is expressed at a modest level, and brain, where it is expressed abundantly. Even though small amounts of ykt6 were present in NRK cells (unpublished data), we chose to limit our detailed analysis to neuron-related cells, where ykt6 staining could be analyzed with confidence. The previous report on rat ykt6 obtained their cDNA from a rat kidney cDNA library, consistent with at least a minor expression level in rat kidney, as we observed in Figure 3. We cannot, however, readily explain the previous findings with ykt6 on liver membranes, because with our antibodies against ykt6, we could not detect ykt6 in rat liver fractions by immunoblotting (Figure 3 and unpublished data). Although we could not detect ykt6 in liver, it is possible that it is present at very low levels.

Do rat brain and yeast ykt6 have the same function(s)? Two factors indicate conservation of function between mammalian and yeast ykt6: first, human ykt6 can complement a Ykt6p-depleted strain (McNew et al., 1997), and second, yeast Ykt6p contains targeting information for localization to the specialized ykt6 compartment in PC12 cells (Figure 10). However, several factors point to a more cell-type specific, specialized role for mammalian ykt6, for example, its dramatic enrichment in neurons and apparent lack of expression in liver, a major secretory cell type (Figure 3). In addition, the lack of significant rat ykt6 staining in Golgi or traditional endosomes and lysosomes does not fit with indications that yeast Ykt6p is involved in general biosynthetic transport from the Golgi to the vacuole (McNew et al., 1997; Tsui and Banfield, 2000; Dilcher et al., 2001). As alluded to above, it is possible that rat ykt6 functions analogously to yeast Ykt6p in some cell types but has evolved in addition to this function, a more specialized role in neurons.

What is the function of ykt6 in neurons? Rat ykt6 behaves as a typical vesicle-SNARE in SNARE assembly reactions in vitro (Figure 13), so every indication is that ykt6 functions in a SNARE complex in membrane fusion reactions. Its localization to unusual punctate vesicles in the cytoplasm implies that ykt6 is involved in the fusion of that compartment, or transport vesicles derived from it, with some other membrane, presumably containing the t-SNARE complex to which ykt6 binds under physiological conditions. The identification of the other SNAREs with which ykt6 is associated in brain will thus give an important clue as to what the membrane fusion partner might be. We observed minor overlaps of ykt6 with markers of dense core granules and lysosomes, although the overall patterns of staining was

usually very distinct (Figures 5 and 7). Because we also observed a minor overlap between ykt6 and endocytosed dextrans (Figure 8), there is a good chance that the ykt6 compartment represents a specialized branch of the endocytic pathway or is at least in communication with endosomes and/or lysosomes. Currently, we can only speculate that neurons, because of their remarkably complex pathways of regulated secretion and the membrane remodeling involved in axon and synapse formation and regulation, might have a need for a specialized lysosome-related or dense core granule-related intracellular compartment regulated by ykt6. Presynaptic as well as postsynaptic membranes must undergo cycles of internalization and recycling or degradation (Buckley *et al.*, 2000). In addition, there may be brain-specific protein and lipid degradative pathways. We should also note that just because ykt6 does not significantly colocalize with other markers of the secretory and endosomal pathways, does not mean that the ykt6 membranes constitute a completely distinct and "novel" compartment. At the light level it is not possible to distinguish whether the ykt6-enriched structures were physically continuous with any of the membranes with which it did not apparently colocalize, and it is possible that the ykt6 membranes represent a specific subcompartment within a larger organelle system such as endosomes or lysosomes.

What is the function of the profilin-like amino-terminal domains? One possible role that has been discussed for yeast Ykt6p is downregulation of the SNARE motif and enforcement of binding specificity. However, although the presence of an intact Ykt6p NT domain was required for complementation of a ykt6 deletion strain, mutations that presumably inactivated its potential SNARE regulatory role accelerated in vitro SNARE complex formation by only about threefold (Tochio *et al.*, 2001). Likewise, complete removal of the sec22b amino-terminal domain did not detectably change the rate of SNARE complex formation (Gonzalez *et al.*, 2001). On the other hand, overexpression of the VAMP 7 NT domain inhibited neurite outgrowth in PC12 cells, perhaps by blocking VAMP 7 interactions with Q-SNAREs like SNAP-25 (Martinez-Arca *et al.*, 2000). Thus, the specific functions of the profilin-like amino-terminal domains of sec22b (and its non-SNARE isoforms sec22a and sec22c), VAMP 7 and ykt6 are not well understood. A major hint is provided by Figure 10 of this report, which demonstrates that the ykt6 NT domain is responsible for targeting the protein to its specialized membrane location. Thus, intracellular membrane targeting appears be a major function for the domain, at least for ykt6. Interestingly, although the yeast Ykt6p NT could fully function in mammalian cell ykt6 targeting, other related NT domains could apparently not (Figure 10). Other profilin-like SNARE NT domains may specifically interact with other compartments or perform unrelated functions. Function of the ykt6 NT domain in membrane targeting in no way precludes additional functions in regulation of SNARE complex formation (Tochio *et al.*, 2001); in fact, these two functions could be mechanistically linked such that interaction of the NT domain with the appropriate membrane receptor would regulate its influence on SNARE complex formation.

Ykt6 is an unusual vesicle-SNARE in that it maintains a substantial cytosolic pool. This feature presents special regulatory problems. For example, the extremely hydrophobic prenyl group(s) must be somehow shielded from solvent to maintain protein solubility. Additionally, the SNARE motif of cytosolic ykt6 must not be allowed to interact with membrane-bound SNAREs and inhibit their function in membrane fusion in the ykt6 or other transport steps. We have presented preliminary evidence for conformational regulation of cytosolic ykt6 that would prevent promiscuous SNARE complex formation (Figures 14 and 15). This putative conformational state seemed to be a relatively permanent feature of cytosolic ykt6 that was not readily provided by cytosol in vitro and was retained after multiple purification steps. We speculate that perhaps protein prenylation is required to attain this putative refractory state. If true, this would suggest a novel protein-lipid interaction that would potentially solve two problems simultaneously. Interaction of the ykt6 SNARE motif and/or NT domain with its own prenyl group could produce the refractory cytosolic conformation, which could be both soluble in the cytosol and nonreactive toward other SNAREs. Targeting to the ykt6 compartment by the NT domain could potentially trigger the release of the prenyl group for membrane insertion while freeing the SNARE motif to participate in SNARE complexes. Future more precise studies will reveal whether this hypothetical mechanism explains the observed phenomena.

ACKNOWLEDGMENTS

REFERENCES

Advani, R.J., Yang, B., Prekeris, R., Lee, K.C., Klumperman, J., and Scheller, R.H. (1999). VAMP-7 mediates vesicular transport from endosomes to lysosomes. J. Cell Biol. *146*, 765–776.

Alory, C., and Balch, W.E. (2001). Organization of the Rab-GDI/CHM superfamily: the functional basis for choroideremia disease. Traffic *2*, 532–543.

Antonin, W., Fasshauer, D., Becker, S., Jahn, R., and Schneider, T.R. (2002). Crystal structure of the endosomal SNARE complex reveals common structural principles of all SNAREs. Nat. Struct. Biol. *14*, 14.

Antonin, W., Holroyd, C., Fasshauer, D., Pabst, S., Von Mollard, G.F., and Jahn, R. (2000). A SNARE complex mediating fusion of late endosomes defines conserved properties of SNARE structure and function. EMBO J. *19*, 6453–6464.

Bock, J.B., Klumperman, J., Davanger, S., and Scheller, R.H. (1997). Syntaxin 6 functions in trans-Golgi network vesicle trafficking. Mol. Biol. Cell *8*, 1261–1271.

Bock, J.B., Matern, H.T., Peden, A.A., and Scheller, R.H. (2001). A genomic perspective on membrane compartment organization. Nature *409*, 839–841.

Bonaldo, M.F., Lennon, G., and Soares, M.B. (1996). Normalization and subtraction: two approaches to facilitate gene discovery. Genome Res 6, 791–806.

Borgstahl, G.E., Williams, D.R., and Getzoff, E.D. (1995). 1.4 A structure of photoactive yellow protein, a cytosolic photoreceptor: unusual fold, active site, and chromophore. Biochemistry 34, 6278–6287.

Brickner, J.H., Blanchette, J.M., Sipos, G., and Fuller, R.S. (2001). The Tlg SNARE complex is required for TGN homotypic fusion. J. Cell Biol. 155, 969–978.

Buckley, K.M., Melikian, H.E., Provoda, C.J., and Waring, M.T. (2000). Regulation of neuronal function by protein trafficking: a role for the endosomal pathway. J. Physiol. (Lond). 525, 11–19.

Catchpoole, D.R., and Wanjin, H. (1999). Characterization of the sequence and expression of a Ykt6 prenylated SNARE from rat. DNA Cell Biol 18, 141–145.

Chen, J.W., Murphy, T.L., Willingham, M.C., Pastan, I., and August, J.T. (1985). Identification of two lysosomal membrane glycoproteins. J. Cell Biol. 101, 85–95.

Coco, S. et al. (1999). Subcellular localization of tetanus neurotoxin-insensitive vesicle- associated membrane protein (VAMP)/VAMP7 in neuronal cells: evidence for a novel membrane compartment. J. Neurosci. 19, 9803–9812.

Dilcher, M., Kohler, B., and Fischer von Mollard, G. (2001). Genetic interactions with the yeast Q-SNARE VTI1 reveal novel functions for the R-SNARE YKT6. J. Biol. Chem., 276, 34537–34544.

Fasshauer, D., Antonin, W., Margittai, M., Pabst, S., and Jahn, R. (1999). Mixed and non-cognate SNARE complexes. Characterization of assembly and biophysical properties. J. Biol. Chem. 274, 15440–15446.

Fasshauer, D., Sutton, R.B., Brunger, A.T., and Jahn, R. (1998). Conserved structural features of the synaptic fusion complex: SNARE proteins reclassified as Q- and R-SNAREs. Proc. Natl. Acad. Sci. USA 95, 15781–15786.

Fukuda, R., McNew, J.A., Weber, T., Parlati, F., Engel, T., Nickel, W., Rothman, J.E., and Sollner, T.H. (2000). Functional architecture of an intracellular membrane t-SNARE. Nature 407, 198–202.

Gelb, M., Scholten, J.D., and Sebolt-Leopold, J. (1998). Protein prenylation: from discovery to prospects for cancer treatment. Curr Opin Chem Biol 2, 40–48.

Gonzalez, L.C., Jr., Weis, W.I., and Scheller, R.H. (2001). A novel SNARE N-terminal domain revealed by the crystal structure of Sec22b. J. Biol. Chem. 17, 17.

Guan, K.L., and Dixon, J.E. (1991). Eukaryotic proteins expressed in Escherichia coli: an improved thrombin cleavage and purification procedure of fusion proteins with glutathione S-transferase. Anal Biochem 192, 262–267.

Hamprecht, B. (1977). Structural, electrophysiological, biochemical, and pharmacological properties of neuroblastoma-glioma cell hybrids in cell culture. Int. Rev. Cytol.49, 99–170.

Hay, J.C. (2001). SNARE complex structure and function. Exp. Cell Res. 271, 10–21.

Hay, J.C., Chao, D.S., Kuo, C.S., and Scheller, R.H. (1997). Protein interactions regulating vesicle transport between the endoplasmic reticulum and Golgi apparatus in mammalian cells. Cell 89, 149–158.

Hay, J.C., Klumperman, J., Oorschot, V., Steegmaier, M., Kuo, C.S., and Scheller, R.H. (1998). Localization, dynamics, and protein interactions reveal distinct roles for ER and Golgi SNAREs. J. Cell Biol. 141, 1489–1502.

Hirling, H., Steiner, P., Chaperon, C., Marsault, R., Regazzi, R., and Catsicas, S. (2000). Syntaxin 13 is a developmentally regulated SNARE involved in neurite outgrowth and endosomal trafficking. Eur J. Neurosci. 12, 1913–1923.

Ho, Y.S., Burden, L.M., and Hurley, J.H. (2000). Structure of the GAF domain, a ubiquitous signaling motif and a new class of cyclic GMP receptor. EMBO J. 19, 5288–5299.

Lafont, F., Verkade, P., Galli, T., Wimmer, C., Louvard, D., and Simons, K. (1999). Raft association of SNAP receptors acting in apical trafficking in Madin-Darby canine kidney cells. Proc. Natl. Acad. Sci. USA 96, 3734–3738.

Liu, Y., and Barlowe, C. (2002). Analysis of Sec22p in ER/Golgi Transport Reveals Cellular Redundancy in SNARE Protein Function. Mol. Biol. Cell 13, 3314–3324.

Lupashin, V.V., Pokrovskaya, I.D., McNew, J.A., and Waters, M.G. (1997). Characterization of a novel yeast SNARE protein implicated in Golgi retrograde traffic. Mol. Biol. Cell 8, 2659–2676.

Martinez-Arca, S., Alberts, P., Zahraoui, A., Louvard, D., and Galli, T. (2000). Role of tetanus neurotoxin insensitive vesicle-associated membrane protein (TI-VAMP) in vesicular transport mediating neurite outgrowth. J. Cell Biol. 149, 889–900.

McNew, J.A., Sogaard, M., Lampen, N.M., Machida, S., Ye, R.R., Lacomis, L., Tempst, P., Rothman, J.E., and Sollner, T.H. (1997). Ykt6p, a prenylated SNARE essential for endoplasmic reticulum-Golgi transport. J. Biol. Chem. 272, 17776–17783.

Mullock, B.M. et al. (2000). Syntaxin 7 is localized to late endosome compartments, associates with Vamp 8, and Is required for late endosome-lysosome fusion. Mol. Biol. Cell 11, 3137–3153.

Nakamura, N., Yamamoto, A., Wada, Y., and Futai, M. (2000). Syntaxin 7 mediates endocytic trafficking to late endosomes. J. Biol. Chem. 275, 6523–6529.

Prekeris, R., Klumperman, J., Chen, Y.A., and Scheller, R.H. (1998). Syntaxin 13 mediates cycling of plasma membrane proteins via tubulovesicular recycling endosomes. J. Cell Biol. 143, 957–971.

Prekeris, R., Klumperman, J., and Scheller, R.H. (2000). Syntaxin 11 is an atypical SNARE abundant in the immune system. Eur. J. Cell Biol. 79, 771–780.

Prekeris, R., Yang, B., Oorschot, V., Klumperman, J., and Scheller, R.H. (1999). Differential roles of syntaxin 7 and syntaxin 8 in endosomal trafficking. Mol. Biol. Cell 10, 3891–3908.

Scales, S.J., Chen, Y.A., Yoo, B.Y., Patel, S.M., Doung, Y.C., and Scheller, R.H. (2000). SNAREs contribute to the specificity of membrane fusion. Neuron 26, 457–464.

Scales, S.J., Pepperkok, R., and Kreis, T.E. (1997). Visualization of ER-to-Golgi transport in living cells reveals a sequential mode of action for COPII and COPI. Cell 90, 1137–1148.

Scales, S.J., Yoo, B.Y., and Scheller, R.H. (2001). The ionic layer is required for efficient dissociation of the SNARE complex by alpha-SNAP and NSF. Proc. Natl. Acad. Sci. USA 98, 14262–14267.

Simonsen, A., Gaullier, J.M., D'Arrigo, A., and Stenmark, H. (1999). The Rab5 effector EEA1 interacts directly with syntaxin-6. J. Biol. Chem. 274, 28857–28860.

Simpson, F., Peden, A.A., Christopoulou, L., and Robinson, M.S. (1997). Characterization of the adaptor-related protein complex, AP-3. J. Cell Biol. 137, 835–845.

Sogaard, M., Tani, K., Ye, R.R., Geromanos, S., Tempst, P., Kirchhausen, T., Rothman, J.E., and Sollner, T. (1994). A rab protein is required for the assembly of SNARE complexes in the docking of transport vesicles. Cell 78, 937–948.

Sollner, T., Whiteheart, S.W., Brunner, M., Erdjument-Bromage, H., Geromanos, S., Tempst, P., and Rothman, J.E. (1993). SNAP receptors implicated in vesicle targeting and fusion. Nature *362*, 318–324.

Steegmaier, M., Oorschot, V., Klumperman, J., and Scheller, R.H. (2000). Syntaxin 17 is abundant in steroidogenic cells and implicated in smooth endoplasmic reticulum membrane dynamics. Mol. Biol. Cell *11*, 2719–2731.

Sutton, R.B., Fasshauer, D., Jahn, R., and Brunger, A.T. (1998). Crystal structure of a SNARE complex involved in synaptic exocytosis at 2.4 A resolution. Nature *395*, 347–353.

Tochio, H., Tsui, M.M., Banfield, D.K., and Zhang, M. (2001). An autoinhibitory mechanism for nonsyntaxin SNARE proteins revealed by the structure of Ykt6p. Science. 293 *698–702,*.

Tsui, M.M., and Banfield, D.K. (2000). Yeast Golgi SNARE interactions are promiscuous. J. Cell Sci. *113* (Pt 1), 145–152.

Ungermann, C., von Mollard, G.F., Jensen, O.N., Margolis, N., Stevens, T.H., and Wickner, W. (1999). Three v-SNAREs and two t-SNAREs, present in a pentameric cis-SNARE complex on isolated vacuoles, are essential for homotypic fusion. J. Cell Biol. *145*, 1435–1442.

Wade, N., Bryant, N.J., Connolly, L.M., Simpson, R.J., Luzio, J.P., Piper, R.C., and James, D.E. (2001). Syntaxin 7 complexes with mouse Vps10p tail interactor 1b, syntaxin 6, vesicle-associated membrane protein (VAMP)8, and VAMP7 in B16 melanoma cells. J. Biol. Chem. *276*, 19820–19827.

Ward, D.M., Pevsner, J., Scullion, M.A., Vaughn, M., and Kaplan, J. (2000). Syntaxin 7 and VAMP-7 are soluble *N*-ethylmaleimide-sensitive factor attachment protein receptors required for late endosome-lysosome and homotypic lysosome fusion in alveolar macrophages. Mol. Biol. Cell *11*, 2327–2333.

Weber, T., Zemelman, B.V., McNew, J.A., Westermann, B., Gmachl, M., Parlati, F., Sollner, T.H., and Rothman, J.E. (1998). SNAREpins: minimal machinery for membrane fusion. Cell *92*, 759–772.

Witters, L.A., Watts, T.D., Gould, G.W., Lienhard, G.E., and Gibbs, E.M. (1988). Regulation of protein phosphorylation by insulin and an insulinomimetic oligosaccharide in 3T3–L1 adipocytes and Fao hepatoma cells. Biochem. Biophys. Res. Commun. *153*, 992–998.

Wong, S.H., Xu, Y., Zhang, T., and Hong, W. (1998). Syntaxin 7, a novel syntaxin member associated with the early endosomal compartment. J. Biol. Chem. *273*, 375–380.

Xu, D., Joglekar, A.P., Williams, A.L., and Hay, J.C. (2000). Subunit structure of a mammalian ER/Golgi SNARE complex. J. Biol. Chem. *275*, 39631–39639.

Yang, B., Gonzalez, L., Jr., Prekeris, R., Steegmaier, M., Advani, R.J., and Scheller, R.H. (1999). SNARE interactions are not selective. Implications for membrane fusion specificity. J. Biol. Chem. *274*, 5649–5653.

Zeng, Q., Subramaniam, V.N., Wong, S.H., Tang, B.L., Parton, R.G., Rea, S., James, D.E., and Hong, W. (1998). A novel synaptobrevin/VAMP homologous protein (VAMP5) is increased during in vitro myogenesis and present in the plasma membrane. Mol. Biol. Cell *9*, 2423–2437.

Zhang, T., and Hong, W. (2001). Ykt6 forms a SNARE complex with syntaxin 5, GS28 and Bet1 and participates in a late stage in ER-Golgi transport. J. Biol. Chem. *276*, 27480–27487.